UNIVERSITY OF CALIFORNIA

Santa Barbara

Estimating Urban Gross Primary Productivity at High Spatial Resolution

A Thesis submitted in partial satisfaction of the

requirements for the degree Master of Arts

in Geography

by

David Lauchlin Miller

Committee in charge:

Professor Joseph P. McFadden, Chair

Professor Dar A. Roberts

Professor Keith C. Clarke

June 2017

The thesis of David Lauchlin Miller is approved.

_____
Dar A. Roberts

_____
Keith C. Clarke

_____
Joseph P. McFadden, Committee Chair

June 2017

Estimating Urban Gross Primary Productivity at High Spatial Resolution

by

David Lauchlin Miller

ACKNOWLEDGEMENTS

The field measurements at KUOM were funded by a grant from the NASA Earth Science Division (NNG04GN80G) as a component of the North American Carbon Program (NACP) and the acquisition of WorldView-2 imagery was funded by a grant from the NSF Coupled Natural and Human Systems program (NSF-0908549).

Special thanks to Emily Peters and Olaf Menzer for organizing all of the in situ measurements; John Potapenko and Bodo Bookhagen for processing the digital surface model and canopy height model from the lidar point clouds; Mike Dolbow at the Minnesota Department of Natural Resources for the help with extracting the leaf-off orthophotos; Yang Lin for his guiding GEOG 214A project; Erin Wetherley for all the help on plots, writing, posters, etc.; Dar Roberts and Keith Clarke for great feedback, comments, and helpful resources; and Joe McFadden for being extraordinarily helpful with nearly every aspect of this project.

Dedicated to Melvin Ephraim Jenkins

ABSTRACT

Estimating Urban Gross Primary Productivity at High Spatial Resolution

by

David Lauchlin Miller

Gross primary productivity (GPP) is an important metric of ecosystem function and is the primary way carbon is transferred from the atmosphere to the land surface. Remote sensing techniques are commonly used to estimate regional and global GPP for carbon budgets. However, urban areas are typically excluded from such estimates due to a lack of parameters specific to urban vegetation and the modeling challenges that arise in mapping GPP across heterogeneous urban land cover. In this study, we estimated typical midsummer GPP within and among vegetation and land use types in the Minneapolis-Saint Paul, Minnesota metropolitan region by deriving light use efficiency parameters specific to urban vegetation types using in situ flux observations and WorldView-2 high spatial resolution satellite imagery. We produced a land cover classification using the satellite imagery, canopy height data from airborne lidar, and leaf-off color-infrared aerial orthophotos, and used regional GIS layers to mask certain land cover/land use types. The classification for built-up and vegetated urban land cover classes distinguished deciduous trees, evergreen trees, turf grass, and golf grass from impervious and soil surfaces, with an overall classification accuracy of 80% (kappa = 0.73). The full study area had 52.1% vegetation cover. The light use efficiency for each vegetation class, with the exception of golf grass, tended to be low

compared to natural vegetation light use efficiencies in the literature. The mapped GPP estimates were within 11% of estimates from independent tall tower eddy covariance measurements. The order of the mapped vegetation classes for the full study area in terms of mean GPP from lowest to highest was: deciduous trees (2.52 gC m^{-2} d^{-1}), evergreen trees (5.81 gC m^{-2} d^{-1}), turf grass (6.05 gC m^{-2} d^{-1}), and golf grass (11.77 gC m^{-2} d^{-1}). Turf grass GPP had a larger coefficient of variation (0.18) than the other vegetation classes (~0.10). Mean land use GPP for the full study area varied as a function of percent vegetation cover. Urban GPP in general, both including and excluding non-vegetated areas, tended to be low relative to natural forests and grasslands. Our results demonstrate that, at the scale of neighborhoods and city blocks within heterogeneous urban landscapes, high spatial resolution GPP estimates are valuable to develop comparisons such as within and among vegetation cover classes and land use types.

TABLE OF CONTENTS

I. Introduction

Gross primary productivity (GPP) is the sum of photosynthesis at the ecosystem scale (Chapin et al., 2002). It is the primary way carbon is transferred from the atmosphere to the land surface, describing the initial inputs of carbon to ecosystems, and is an important metric of ecosystem function (Heinsch et al., 2006). Models of GPP from satellite remote sensing have proven to be useful for monitoring carbon uptake at regional-to-global scales, providing improved constraints on temporal and spatial patterns across many biomes (e.g., Running et al., 2004). However, urban areas are often not included in such large-scale models due to the small percentage of the global land area covered by cities relative to the major natural biomes.

There is a distinct need for mapping GPP within urban areas because it is relatively unknown how GPP varies among vegetation and land use types in these regions. More than half of the global population lives in urban areas, and this proportion is expected to grow through the 21st century (Grimm et al., 2008). Urbanization increases impervious surface cover, which results in stronger urban heat islands (Imhoff et al., 2010) and intensified runoff (Burian and Pomeroy, 2010), and it also replaces native vegetation, negatively affecting terrestrial carbon storage (Seto et al., 2012). Once established, urban vegetation can provide many ecosystem services including local cooling (Oke, 1989) and absorption of airborne pollutants (Nowak et al., 2006). Urban vegetation has direct effects on urban carbon budgets through CO_2 uptake and storage and also indirect effects by reducing energy use due to shading and windbreaks, as well as potentially increased fossil fuel consumption for maintenance (Pataki et al., 2006). Field surveys are often done to provide estimates of carbon cycling of urban vegetated surfaces, but such surveys are time-consuming and

require robust spatial sampling to accurately scale to the entire urban extent (e.g., Nowak & Crane, 2002; Nowak et al., 2008).

Remote sensing of GPP in urban areas is more repeatable and spatially explicit while being less work-intensive than field surveys. The goal of many urban remote sensing studies of GPP and net primary productivity (NPP = GPP – plant respiration) is to quantify the change in primary production as a result of urban development (e.g. Imhoff et al., 2000; Imhoff et al., 2004; Xu et al., 2007; Buyantuyev and Wu, 2009; Lu et al., 2010; Pei et al., 2013). In general, urban development reduces primary production in densely vegetated regions (Imhoff et al., 2004), but can increase primary production in some areas previously covered by agriculture (Zhao et al., 2007) or deserts (Buyantuyev and Wu, 2009).

One of the most established methods to calculate GPP from remote sensing is the light use efficiency (LUE) approach, and it was first proposed by Monteith in 1972 (Verma et al., 2015; Ma et al., 2014). The LUE technique is based on the assumption that vegetation converts absorbed photosynthetically active radiation (PAR) at a certain rate, or LUE. As such, GPP can be calculated as:

$$GPP = FPAR * PAR * LUE$$

where GPP is the mass of carbon taken up in the pixel area over a period of time (e.g., $gC\ m^{-2}\ d^{-1}$), PAR is the incident photosynthetically active radiation received in the pixel area over a period of time (e.g., $MJ\ m^{-2}\ d^{-1}$), FPAR is the unitless fraction of PAR absorbed by the vegetated surface within the pixel, and LUE is the conversion rate from absorbed PAR to carbon uptake (e.g., $gC\ MJ^{-1}$) (Heinsch et al., 2003). Versions of this method have been used

in many models to estimate large-scale dynamics of GPP, such as GLO-PEM (Prince & Goward, 1995), CASA (Potter et al., 1993), VPM (Xiao et al., 2004), and MODIS GPP (MOD17) (Running et al., 2004), and there have been many comparisons between the models and flux measurements (e.g. Running et al., 1999; Turner et al., 2003a; Yuan et al., 2007; Xiao et al., 2010; Ogutu and Dash, 2013; Verma et al., 2015). FPAR is often estimated through spectral vegetation indices (e.g. Myneni and Williams, 1994; Mahadevan et al., 2008) and radiative transfer modeling (e.g. Knyazikhin et al., 1999; Myneni et al., 2002) (Song et al., 2013; D'Odorico et al., 2014). LUE varies by species and the environmental conditions affecting an individual plant (Ahl et al., 2004; Schwalm et al., 2006), but has been successfully modeled by plant functional type at a variety of scales (Goetz & Prince, 1999; Turner et al., 2005; Verma et al., 2014).

GPP estimates from remote sensing are typically validated using field survey or flux tower data and typically in using the LUE approach each image pixel is labeled as a unique vegetation class to scale to the ecosystem level due to differences in physiological and functional characteristics (Chapin, 1993; Ruimy et al., 1994; Heinsch et al., 2006; Reich et al., 2012). This is a challenge in urban areas for the remote sensing systems typically used to estimate GPP at regional and global scales (e.g. Landsat TM and MODIS) because their spatial resolutions are too coarse to readily distinguish small patches of vegetation, such as street trees, from surrounding urban structures, such as roads and buildings (Raciti et al., 2014). Mixed pixels contain multiple surfaces that reflect incident radiation at different magnitudes and directions. This modifies the FPAR value of the pixel and makes it difficult to estimate and ascribe LUE values uniquely to each vegetation type within a pixel. The MODIS GPP product (MOD17), for example, applies LUE parameters by classifying the

vegetated land surface into a few dominant biome classes, but does not include a LUE parameter for urban areas (Running and Zhao, 2015).

Urban areas have highly variable surface cover over relatively short distances (Cadenesso et al., 2007; Woodcock and Strahler, 1987), thus distinguishing among vegetation types and other surfaces is often approached using imagery with either high spectral resolution or high spatial resolution. Hyperspectral imagery (high spectral resolution) and techniques such as spectral mixture analysis (e.g. MESMA, Roberts et al., 1998) can reliably map many urban materials (Herold et al., 2003), contributions of within-pixel reflectance of different surface types (Wetherley et al., 2017), and tree species when combined with lidar (Alonzo et al., 2014). However, imagery with high spatial resolution is much more commonly available and is generally more amenable to mutually exclusive classification of surface features when subtle spectral differences are of less importance, either with pixel- or object-based techniques (e.g. Myeong et al., 2001; Myint et al., 2011; Nouri et al., 2014). A significant issue is that it can be difficult to separate trees from grasses due to their spectral similarity using only multispectral, high resolution imagery (Myeong et al., 2001; Walton et al., 2008), but lidar data can be used as an additional input in order to distinguish vegetation types by height (e.g. Raciti et al., 2014). Such data is often of limited availability, and has not yet been applied to urban primary production studies.

In urban GPP studies, the issue of small-scale surface heterogeneity tends to be approached by assigning estimates of fractional cover to each pixel (e.g. Zhao et al., 2007; Zhao et al., 2012), by considering urban areas as a single vegetation type (such as savanna) in which condition varies as a function of a vegetation index (e.g. Milesi et al., 2003), or by using relatively high spatial resolution imagery to better separate vegetated and non-

vegetated surfaces (As-syakur et al., 2010; Wu and Bauer, 2012). More recent work has been done to estimate urban biogenic fluxes as they vary with impervious surface cover, urban heat island, and plant phenology (Hardiman et al., 2017). However, most studies use LUE values from natural ecosystems for urban vegetation (e.g. Zhao et al., 2007) because there have been few field measurements of LUE in cities (e.g. Wu and Bauer, 2012). Due to data availability and scale, variability of urban primary production by land cover type is often analyzed using large pixels (e.g. Imhoff et al., 2000; Zhao et al., 2007), and it is still unclear how different vegetation and land use types individually affect GPP within urbanized areas at a scale in which lawns, trees, and roads can be identified. In general, the importance of unique parameterization of urban vegetation cover types in order to accurately characterize urban GPP is still relatively unknown.

Here, we used high resolution surface reflectance data from WorldView-2 (WV-2) satellite imagery to estimate GPP across the Minneapolis-Saint Paul, Minnesota metropolitan area. We produced a land cover classification using the WV-2 imagery, canopy height data from airborne lidar, and leaf-off color-infrared aerial orthophotos, and used regional GIS layers to mask specific land cover/land use types. We calculated empirical LUE estimates for deciduous trees, evergreen trees, turf grass, and golf grass from WV-2 reflectance by using in situ observations of GPP from eddy covariance and tree sap flow. We compared our mapped GPP estimates using eddy covariance observations at 40 m height from a tall tower (KUOM) near our in situ training sites, and we assessed the variability of GPP by vegetation and land use type across the study area. These results help contextualize urban GPP in relation to larger-scale satellite remote sensing estimates and natural ecosystems.

Our main research questions were the following:

1. What is the magnitude and variability of GPP within dominant urban vegetation types, specifically deciduous trees, evergreen trees, turf grass, and golf grass?
2. What is the magnitude and variability of GPP within major urban land use types? Is land use GPP more determined by percent vegetation cover or by GPP variability within vegetation types?
3. How does urban vegetation GPP compare to natural vegetation, and what are likely urban vegetation NPP estimates based on our data and local knowledge?

II. Methods

A. Study Area

Our study site was a large area (894 km^2) of the Minneapolis-Saint Paul, Minnesota (~ 44° 59' N, 93° 11' W) metropolitan region. The region has a humid, temperate continental climate with warm summers and very cold winters, and receives precipitation year-round. As described in Peters et al. (2011), the region has a mean annual temperature of 7.4° C and mean annual precipitation of 747 mm. It has two densely developed urban cores approximately 14 km apart surrounded by extensive suburban residential development, and much of the study area is likely to be influenced by the urban heat island effect (Winkler et al., 1981, Todhunter, 1996; Sen Roy & Yuan, 2009). The Twin Cities region has been undergoing urban growth and expansion, and is expected to grow by over 800 000 people between 2010 and 2040 (Metropolitan Council, 2016; Yuan et al., 2005).

We selected this region due to the availability of in situ observations of GPP from sap flux, leaf-level gas exchange, and eddy covariance for dominant urban vegetation types in the region: deciduous trees, evergreen trees, and turf grass. All deciduous trees were broadleaf, and all evergreen trees were needleleaf. Common deciduous trees included ash (*Fraxinus sp.*), elm (*Ulmus sp.*), red oak (*Quercus rubra*), eastern black walnut (*Juglans nigra*), and American basswood (*Tilia Americana*), common evergreen trees included spruce (*Picea sp.*) and pine (*Pinus sp.*) (Peters and McFadden, 2012), and common turf grass species included Kentucky bluegrass (*Poa pratensis* L.), tall fescue (*Festuca arundinacea* Schreb.), and perennial ryegrass (*Lolium perenne* L.) (Hiller et al., 2011). The eddy covariance measurements were made at 40 m height on a tall radio tower (KUOM) near the in situ observations of trees and turf grass in order to compare with our mapped GPP estimates (Peters and McFadden, 2012; Menzer et al., 2015).

B. Land Cover Classification and Validation

We used a digital surface model (DSM) as a basemap for orthorectification and image alignment, and a canopy height model (CHM) to estimate tree height, both at 1 m spatial resolution and derived from lidar data. Fugro Horizons, Inc. and the Minnesota Department of Natural Resources (MN DNR) collected the multi-return lidar point cloud data during 2011 and 2012 at various point densities (Fugro Horizons, Inc. and the Minnesota Department of Natural Resources, 2015). A Leica sensor ALS50-II MPiA acquired at a point density of 1.5 points m^{-2}, and a FLI-MAP sensor acquired at point densities of 2 and 8 points m^{-2} in different regions. Gridded rasters of the lidar data were

created with custom Python scripts that used components of LAStools (rapidlasso GmbH – Gilching, Germany) (Potapenko, 2014).

We used imagery from WV-2 as the basis for our GPP analysis. WV-2 provided 2 m spatial resolution in eight multispectral bands in the visible and NIR (Digital Globe, 2013) on the dates of July 17, 2010 and July 28, 2010. We converted the raw WV-2 digital numbers to radiance, and orthorectified them using 16 ground control points (GCPs) referenced to the DSM and rational polynomial coefficient files provided by Digital Globe. We atmospherically corrected the orthorectified WV-2 images with the Fast Line-of-sight Atmospheric Analysis of Hypercubes (FLAASH) add-on in ENVI Classic (Adler-Golden et al., 1998). We mosaicked the surface reflectance images into a single image and assessed its spatial alignment with the DSM. Prior to resampling, most of the mosaic had <4 m shift compared to the DSM. Then, we resampled the WV-2 mosaic to 1 m and aligned it with the DSM base map using a nearest neighbor approach and a first degree polynomial fit with 113 GCPs. The resulting average RMSE (100 targets) with the DSM base map was 1.69 m, with a standard deviation of 0.79 m, less than the original 2 m resolution of the WV-2 imagery. The warped WV-2 images were then clipped to form a final mosaic (NAD83, UTM Zone 15N).

To initially distinguish vegetated and non-vegetated pixels, we used a maximum likelihood classifier, using all of the WV-2 bands and the Normalized Difference Vegetation Index (NDVI) (Tucker, 1979). We calculated NDVI using the NIR1 and red bands of WV-2. We chose the NIR1 band rather than NIR2 because the former had more similar spectral coverage to the NIR bands in Landsat Thematic Mapper and MODIS. The maximum likelihood classifier is a supervised classification method that assumes a normal distribution

for each of the input spectral bands, and selects the best class for a given pixel based on probability (Jia and Richards, 1994). We did not limit the probability threshold, and classified all pixels. We captured the training data using regions of interest (ROIs) with a total of approximately 84 000 pixels at 1 m spatial resolution chosen for each class, selecting a new polygon in each cell of a 5 km grid overlaid on the image. Non-vegetated pixels included roads, buildings, bare soil, and other built surfaces. Vegetation included all trees, grasses, shrubs, and other plants. Water was masked, and we labeled lakes and rivers using a modified version of an open water bodies GIS layer from the Metropolitan Council (2013). We chose not to spectrally classify water bodies to avoid confusion with building and tree shadows, and also to prevent mislabeling of algae-covered water bodies as land vegetation.

The initial WV-2 NDVI had a small offset between the two images, and we corrected this by selecting ROIs of both vegetated and non-vegetated surfaces in the overlapping region of the images. We used the average NDVI value of a given ROI to reduce the possible effects of pixel shifts. For each ROI, we regressed the NDVI value for the July 17, 2010 image to the July 28, 2010 image because July 28 had fewer clouds than July 17 and our in situ sites were located within the July 28 image. The NDVI values for the July 17 area of the image mosaic were adjusted using this regression ($NDVI_{July\ 28} = 1.0246 * NDVI_{July\ 17} + 0.0040$, $R^2 = 0.9869$, $p < 0.001$). After adjustment, there was no longer an apparent difference in NDVI between the two halves of the mosaic.

To separate the vegetation into trees and turf grass classes, we used a 1 m height threshold based on the CHM, following Raciti et al. (2014). Vegetation pixels greater than 1 m in height were classified as trees, and the remainder as turf grass. We found the CHM contained gaps of missing pixels within our tree canopy, but we were able to remove these

canopy gaps and better express tree cover using a 3x3 mean filter after classifying with the CHM. We also relabeled as turf grass some areas of power and transmission lines that had been misclassified as trees.

To distinguish golf grass and turf grass, we used the original version of the Generalized Land Use 2010 GIS layer (Metropolitan Council, 2011). We labeled any turf grass pixel within the golf course land use extent to be golf grass, with all remaining grass as turf grass. We separated these classes because golf grass had a much higher level of maintenance than ordinary turf grass, and thus required a different parameterization for the GPP calculation.

To separate deciduous and evergreen trees, we relied on color infrared digital orthophotos acquired during leaf-off conditions. The Minnesota Department of Natural Resources (MN DNR) and Surdex Corporation acquired the imagery during April 2010 at 0.3 m resolution (Minnesota Department of Natural Resources and Surdex Corporation, 2015). We resampled the imagery to 1 m resolution and aligned it to our DSM (mean RMSE = 2.028 m). We selected separate ROIs for deciduous and evergreen trees from the existing tree class using the WV-2 imagery, the aligned leaf-off orthophoto, and Google Earth, and we extracted the WV-2 NDVI and the leaf-off NDVI for these locations. We assessed the separability of the classes based on the leaf-off NDVI alone and an NDVI ratio: leaf-off NDVI / WV-2 NDVI. We found a threshold of 0.4638 of the NDVI ratio was more reliable than the leaf-off NDVI alone. After applying the threshold, we used a 5x5 median filter within the tree classes to remove misclassified pixels.

To label wetlands, we used a wetlands and wet areas GIS layer from the Metropolitan Mosquito Control District (2012). We did not want to include wetlands in our

GPP calculation because they have very different physiological characteristics from grass (Chapin et al., 2002), and we did not have in situ observations of wetland GPP available. This layer included many types of wetlands, and we did not include well-drained grasses and woodlands (type 1) in the wetland class. We added and modified some of the wetlands layer's polygons based on our WV-2 imagery, and we replaced turf grass and impervious and soil pixels within the modified wetland layer's boundaries.

To label agriculture, we used a modified version of the Generalized Land Use 2010 GIS layer from the Metropolitan Council (2011), and the agriculture class replaced any class that was previously present in its location. We manually adjusted the boundaries of the agriculture class using the WV-2 imagery as a reference in a few areas of the study area where this class overlapped roads or trees.

Lastly, we identified and masked clouds and cloud shadows by manually creating polygons using the NDVI and a red-rededge-green RGB display from WV-2.

We assessed the accuracy of our land cover classification for the built-up and urban vegetation classes, namely deciduous trees, evergreen trees, grass (turf + golf), and impervious and soil. For classification accuracy assessment turf and golf grass were treated as a single class, called grass (= turf grass + golf grass). We randomly sampled 100 initial pixel targets for each of the four land cover classes, and we assessed each of the targets using the WV-2 imagery, a 1 ft (0.3 m) spatial resolution RGB USGS orthophoto acquired in early spring 2012, and Google Earth. We excluded targets that were difficult to label, resulting in 275 evaluated targets.

C. NDVI and FPAR

We calculated FPAR based on the adjusted WV-2 NDVI using the relationship from Sims et al. (2006a):

$$FPAR = 1.24 * NDVI – 0.168.$$

This relationship was based on ground measurements of various plant functional types, and has been used in previous studies based on MODIS NDVI (e.g. Wu et al., 2012; Zhang et al., 2016). It is similar to many other NDVI-FPAR linear relationships that exist in the literature (Ruimy et al., 1994; Song et al., 2013).

To use this relationship appropriately, we needed to convert the adjusted WV-2 NDVI to a MODIS-like NDVI, which could then be used to estimate FPAR. For example Zhao et al. (2007) used AVHRR NDVI, which was multiplied by 1.45 (Huete et al., 2002) before it could be used with the MODIS backup NDVI-FPAR look up table (Knyazikhin et al., 1999). We did not find such a relationship for WV-2 and MODIS NDVI in the literature, thus we developed our own empirical relationship. To do so, we needed to compare how WV-2 and MODIS NDVI would appear under identical acquisition conditions. We used an Airborne Visible/Infrared Imaging Spectrometer (AVIRIS) image from July 29, 2009 of Rosemount, Minnesota. We atmospherically corrected the AVIRIS radiance image with ACORN 6.080101 mode 1.5 to create land surface reflectance image using a summer atmospheric model, derived water vapor at 940 nm, and 50 km image atmosphere visibility (ImSpec LLC – Palmdale, CA, USA). AVIRIS has 224 bands at 10 nm spacing across the visible and shortwave near infrared (Green et al., 1998), and we used the spectral response functions of WV-2 and MODIS in ENVI 5.1 to resample the AVIRIS reflectance image to the band passes of these sensors to develop approximate WV-2 and MODIS reflectance

images. We produced an NDVI image for each of these sensor types based on the AVIRIS image.

We used every available pixel in the AVIRIS image extent to produce linear regressions between the resampled WV-2 and MODIS NDVIs. We found there were several linear relationships present between the resampled MODIS NDVI and the resampled WV-2 NDVI due to differences in the spectral placement of the red and NIR bands in the sensors, and these varying linear relationships were attributable to land cover types within the extent of the AVIRIS image. Specifically, we found that the surfaces below the line of $NDVI_{MODIS} = 1.01 * NDVI_{WV-2} - 0.025$ were almost always water surfaces, while those above the line were impervious surfaces, soils, and vegetation. We masked all pixels below this line, and then developed a regression from the remaining pixels: $NDVI_{MODIS} = 0.9842 * NDVI_{WV-2} + 0.01039$; $R^2 = 0.9994$. We used this regression to convert our adjusted WV-2 NDVI to our best approximation of a MODIS NDVI, which was then used in the equation from Sims et al. (2006a) to produce an image of FPAR for the study area.

D. In Situ CO_2 Flux Data and Light Use Efficiency Estimation

We used in situ observations of GPP and PAR to derive an empirical light use efficiency (LUE) estimate for each vegetation type. Tree GPP was based on sap flow and leaf-level gas exchange, and turf grass GPP was based on eddy covariance, both at half hourly intervals. The in situ observations were in a first-ring suburban neighborhood in the center of our study area (Peters and McFadden, 2012).

Sap flow and leaf-level gas exchange measurements are described in Peters et al. (2010) and Peters and McFadden (2012), and were collected during 2007 and 2008 on trees

in park-like conditions. Maintenance was considered to be low at all tree sites, with no irrigation, no fertilizer, and regular mowing. Peters and McFadden (2012) calculated whole tree transpiration using sap flow techniques, and canopy-level meteorological measurements were used to estimate canopy conductance. Measurements of photosynthesis and stomatal conductance from leaf-level gas exchange measurements were used to estimate canopy photosynthesis (i.e. GPP) from canopy conductance across the growing season. We produced separate GPP estimates for deciduous and evergreen trees by aggregating the sap flux measurements by vegetation type.

Turf grass eddy covariance measurements are described in Hiller et al. (2011), and were acquired during 2005-2009 at a first-ring suburban 1.5 ha cool-season turf grass field site representative of low-maintenance lawns, with regular mowing, no clipping removal, no irrigation, and only one application of fertilizer per year (Peters and McFadden, 2012). Instrumentation included a CR5000 data-logger, a CSAT3 sonic anemometer (both Campbell Scientific, Inc., Logan, Utah, USA), and an open-path infrared gas analyzer (IRGA) (LI-7500, LI-COR, Inc., Lincoln, Nebraska, USA) (Hiller et al., 2011). Measurements were taken using a portable mast tower at 1.35 m height and included CO_2, water vapor, energy fluxes (downwelling and upwelling), and momentum exchange. We calculated PAR for both trees and turf grass using the shortwave radiometer measuring downwelling radiation at the turf grass site multiplied by 0.45 (Heinsch et al., 2003). CO_2 flux data were processed using a version of the eth-flux program, and turf grass vegetation fluxes were separated from traffic fluxes using a multiple regression model to obtain estimates of turf grass GPP (Hiller et al., 2011).

We did not have in situ measurements for golf grass, but Peters and McFadden (2012) modeled GPP for irrigated grass based measurements at the turf grass site during the spring and fall using light-response curves and ecosystem respiration models. These models were then applied to midsummer soil temperature and soil radiation data to estimate irrigated grass GPP during midsummer. We used this modeled estimate for irrigated grass to approximate golf grass GPP. The authors noted that this modeled estimate did not account for fertilization or other benefits of increased maintenance that golf grass would experience, thus it likely represents a conservative value of golf grass GPP.

We summed mean diurnal cycles to estimate typical daily PAR and GPP for our in situ sites in order to characterize typical daily vegetation function for this time of year. Using GPP and PAR estimates at half hourly intervals, we tested 2-week (day of year (DOY) 203-216), 3-week (DOY 199-219), and 4-week (DOY 196-223) intervals centered on July 28 (DOY 209), using only measured (i.e., not gap-filled) data from the turf grass eddy covariance site. We restricted the mean diurnal cycles to be during daylight (PAR > 0.45 W m^{-2}), and we removed erroneous GPP and PAR values due to rainy or cloudy conditions and/or instrument error. Due to hotter and drier conditions in 2007, we chose to use data from only 2008 for trees, and only 2006 and 2008 for turf grass. The years 2006 and 2008 were more representative of typical climate conditions during midsummer in the region. We averaged the remaining data points at each half hour, and then summed them to produce a typical, single day estimate of GPP (gC m^{-2} d^{-1}) and incident PAR (MJ m^{-2} d^{-1}) for the 2, 3, and 4-week intervals. After assessment, we selected the 4-week window for our analysis. The resulting GPP and PAR daily sums were composites to best characterize vegetation function during midsummer.

We extracted polygons in our FPAR image at the in situ observation sites in order to estimate a typical FPAR with which to calculate empirical LUE values. We selected a total of 2899 pixels for deciduous trees and 490 pixels for evergreen trees from all sap flow sites, and we selected a rectangular polygon of 4410 pixels containing the turf grass eddy covariance tower. We were conservative in selecting these polygons, avoiding class boundaries and confirming the cover type with our WV-2 imagery and Google Earth prior to selection. We then calculated the mean FPAR for each vegetation type from the site polygons. Since we did not have a specific site for the golf course FPAR, we used the mean of all golf grass FPAR in the WV-2 imagery extent.

We calculated the empirical LUE for each vegetated surface type using the FPAR estimates from the site polygons, the 4-week reference PAR values for each vegetated surface, and the 4-week reference GPP values. Empirical LUE was calculated as:

$$LUE = GPP / (FPAR * PAR)$$

E. GPP Estimation and Validation

The eddy covariance measurements were made at 40 m height on a tall radio tower (KUOM) that was located within 1 km of both the turf grass and tree sites (Peters and McFadden, 2012; Menzer et al., 2015). We used these data to estimate typical PAR for our GPP map, and to independently compare tower-based GPP to our composite GPP map. For data processing and filtering information, we refer to Peters and McFadden (2012) and Menzer et al. (2015). The tall tower data that we used were summarized at half hourly intervals, and were of high quality based on the following rules: (1) each measurement was from the northwest wind sector (270 degrees < azimuth < 360 degrees); (2) a flux measurement was observed, meaning that none of the data was gap-filled; and (3) we only

used flux observations that had a cumulative source area of greater than 99% within the study area used in Menzer et al. (2015). These restrictions were necessary in order to guarantee the best observations from the tall tower for comparison with our typical composite GPP estimates.

Similar to the tree and turf grass sites, we summed the mean diurnal cycles of the tall tower GPP and PAR data from observations at half hour intervals. We used data during daylight (PAR > 0.45) from 2008, and tested the same weekly intervals as the other in situ data. We had insufficient data points to generate a complete mean diurnal cycle at the 2-week interval for the tall tower, but the 3 and 4-week interval had similar estimates for GPP and PAR. We used the 4-week estimates in order to match the mean diurnal cycles from the tree and turf grass in situ data.

We generated our composite map of GPP by multiplying the FPAR map values by the 4-week PAR from the 40 m tower (12.09 MJ m^{-2} d^{-1}) and the LUE estimates for each vegetation type.

$$GPP = FPAR * PAR * LUE$$

The resulting map represented a composite of typical clear-sky, midsummer conditions, and varied spatially based on the FPAR derived from WV-2 NDVI and the vegetation types from the land cover classification.

We used flux footprint polygons for the tall tower site to compare with our GPP map, and each polygon represented the modeled ground area from which 80% of a given flux measurement originated (Kljun et al., 2004; Velasco and Roth, 2010). We merged the polygons from each of the observations that were selected in generating the 4-week mean diurnal cycle to create a single polygon that represented the ground projected area of the tall

tower flux observations. We extracted the GPP estimates of all vegetated pixels within this polygon, and used the mean value to compare with the tall tower's summed mean diurnal cycle.

We quantified variation in urban GPP by analyzing how GPP varied among and within dominant vegetation types and land use types. Vegetation types that we compared included deciduous trees, evergreen trees, turf grass, and golf grass. Land use types were derived from the Generalized Land Use 2010 GIS layer and included: airport; golf course; industrial; institutional; major highway; mixed use; office; park, recreational, or preserve; residential; retail; and undeveloped.

III. Results

A. Vegetation Classification

Our land cover classification (Figure 1) had an overall accuracy of 80% (kappa = 0.73) for built-up and vegetated urban land cover classes, which included the impervious and soil, deciduous tree, evergreen tree, and grass (turf + golf) classes (Table 1). We did not consider the other land cover classes (water, wetland, agriculture, and clouds) in our accuracy assessment because those classes were mapped primarily from existing GIS data sources rather than our imagery or they were not the focus of our urban GPP analysis.

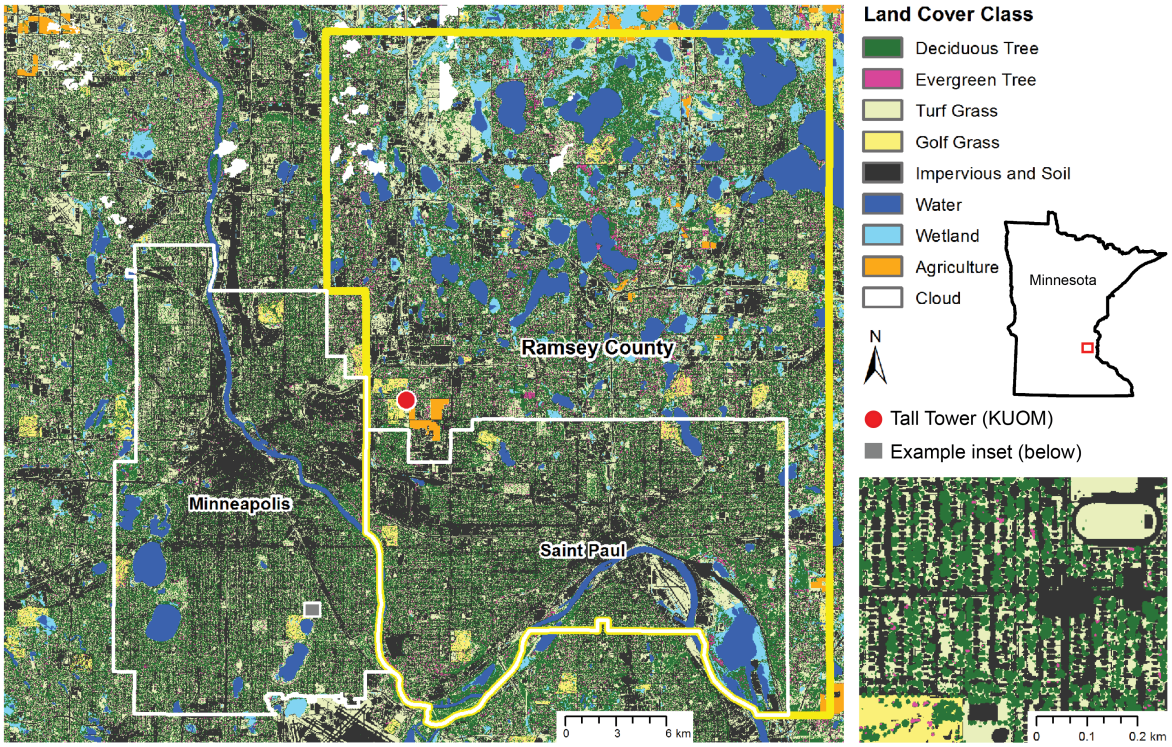

Figure 1: Land cover classification for the full study extent (32 km x 28 km) (left), with the KUOM flux tower location indicated by a red circle, the Minneapolis and Saint Paul boundaries by the white lines, and the Ramsey County boundary by the yellow lines. Subset (lower right) location indicated by gray box. Location of study area in Minnesota indicated by red box in state outline (right).

Table 1: Accuracy assessment table for built-up and vegetated urban land cover classes. Overall accuracy was 80% (kappa = 0.73). Golf and turf grass were considered as one class for accuracy assessment because they were distinguished from one another using a GIS layer rather than the raster image classification.

		Reference					
		Deciduous Tree	Evergreen Tree	Grass (Turf + Golf)	Impervious and Soil	Total	User's Acc.
Classification	Deciduous Tree	54	3	2	0	59	0.92
	Evergreen Tree	33	33	3	1	70	0.47
	Grass (Turf + Golf)	8	0	51	3	62	0.82
	Impervious and Soil	0	0	2	82	84	0.98
	Total	95	36	58	86	275	
	Producer's Acc.	0.57	0.92	0.88	0.95		

We obtained high producer's accuracies for the impervious and soil (0.95), evergreen tree (0.92), and grass (turf + golf) (0.88) classes, and high user's accuracies for the impervious and soil (0.98), deciduous tree (0.92), and grass (turf + golf) (0.82) classes. Most misclassification was between the deciduous and evergreen tree classes. Nearly all real evergreen trees were correctly classified (producer's accuracy = 0.92), but on the map itself, many trees that were classified as evergreen were actually deciduous (user's accuracy = 0.47). Given the leaf off data we had available, we believed it was more important to accurately map every real evergreen tree, resulting in a high producer's accuracy for evergreen trees, due to the very small area of evergreen trees in the image. A consequence was that we misclassified a small amount of the dominant deciduous tree class as evergreen trees.

We also had misclassification between deciduous trees and grass (turf + golf). In our accuracy assessment process, eight targets were classified as turf grass, but were actually deciduous trees. Most of these targets were either at the edge of a tree canopy, in canopy gaps, or consisted of shrubs. This is likely a result of the low pass filter we used to reduce pits and gaps in the tree canopy that originated from using the lidar canopy height raster to distinguish between trees and grasses.

Grouping the vegetation classes together, we had an overall accuracy of 98% (kappa = 0.95) in classifying vegetated versus impervious and soil. Grouping the tree classes and not including the impervious and soil, our classification was able to distinguish both the tree classes from the grass (turf + golf) with an accuracy of 93% (kappa = 0.84). Not including the impervious and soil and evaluating the vegetation classes alone, we obtained an overall accuracy of 74% (kappa = 0.61) in distinguishing between vegetation classes. Evaluating the

tree classes alone and not including the grass (turf + soil) and impervious and soil classes, deciduous trees had user's and producer's accuracies of 95% and 62%, respectively, and evergreen trees had user's and producer's accuracies of 50% and 92%, respectively.

The plan area fractional cover of vegetation and other land cover types are given in Table 2. The vegetation cover of the full study extent was 52.1% including all land cover classes: deciduous tree cover was 25.5%, evergreen tree cover was 2.5%, turf grass cover was 22.9%, and golf grass cover was 1.2%. These are similar to the percent cover estimates for the cities of Minneapolis and Saint Paul, as well as Ramsey County. However, the percentage of impervious and soil surface cover was greater in the cities of Minneapolis and Saint Paul than the background values for the entire study area and Ramsey County.

Table 2: Percent cover of the different land cover types within the full study extent and the administrative boundaries of Minneapolis, Saint Paul, and Ramsey County.

	Full Study Extent	Minneapolis	Saint Paul	Ramsey County
Deciduous Tree	25.5	23.7	26.2	26.4
Evergreen Tree	2.5	1.4	2.3	3.1
Turf Grass	22.9	20.2	19.3	21.8
Golf Grass	1.2	0.9	1.2	1.1
Impervious and Soil	35.5	47.5	42.7	31.8
Water	7.2	6.0	6.6	9.5
Wetland	3.8	0.3	1.7	5.2
Agriculture	0.6	0.0	0.0	0.5
Cloud	0.7	0.0	0.0	0.7

B. FPAR Retrieval

The distribution of FPAR by vegetation type is shown in Figure 2. Deciduous trees, evergreen trees, and golf grass had similarly high FPAR values, while the turf grass had a relatively broader distribution with a lower mean value. The mean FPAR values were 0.87, 0.86, 0.76, and 0.86 for deciduous trees, evergreen trees, turf grass, and golf grass, respectively. The median values were greater than the means, with values of 0.90, 0.87, 0.78, and 0.88 for deciduous trees, evergreen trees, turf grass, and golf grass, respectively. All of the distributions were left skewed, with skewness values of -1.84 for deciduous trees, -1.12 for evergreen trees, -0.71 for turf grass, and -2.07 for golf grass. Turf grass had a greater coefficient of variation (CV) than the other vegetation classes, which were otherwise similar. The CV was 0.10 for deciduous trees, 0.09 for evergreen trees, 0.18 for turf grass, and 0.10 for golf grass.

We selected FPAR values to train the GPP model based on manually delineated regions of interest from the map at the in situ measurement sites, with the exception of the golf grass class. We chose these regions of interest to represent typical FPAR conditions for each of the parameterized vegetation classes in order to pair these data with in situ GPP measurements. We did not have in situ observations of the golf grass GPP, and so we estimated typical golf grass FPAR by using the mean value of all golf grass pixels. Using these polygons and the golf grass mean, the deciduous tree class had the highest FPAR (0.88), and golf grass (0.86) and evergreen trees (0.83) also had high values, while turf grass (0.74) had the lowest. Not including the golf grass, these observed values were all less than the mean FPAR value for each vegetation class, but were less than one-half of the standard deviation from the mean.

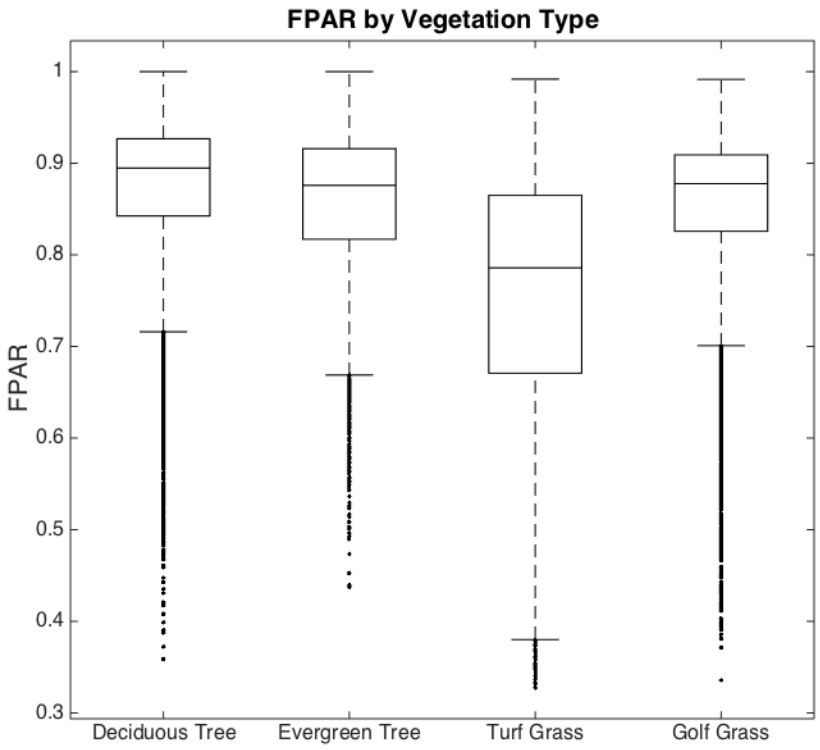

Figure 2: Box plots of FPAR by vegetation type for the full study extent (10000 samples per class). For a given box plot, the middle line of the box is the median, the outer edges of the box are the 25th and 75th percentiles, and dashed lines are whiskers that extend to 1.5 * the standard deviation, with values greater than this from the median shown as dots.

C. Light Use Efficiency Parameters

We estimated typical daily GPP and PAR values by summing mean diurnal cycles from half-hourly data at our in situ measurement sites (Figure 3). These were based on all daytime (PAR > 0.45 W m^{-2}) observations during clear weather conditions during a range of weeks centered on July 28. Within each vegetation type's mean diurnal cycle, we used the same half-hourly time points of GPP and PAR. The deciduous and evergreen tree half-hourly GPP exhibited hysteresis patterns typical of sap flux measurements, with a rapid increase in the morning and slow decline in the afternoon, and deciduous trees reached much lower daily maximum values than evergreen trees. The half-hourly turf grass GPP tended to reach a daily maximum in the mid-morning that remained relatively constant until the late afternoon, depending on weather conditions. The modeled golf grass GPP did not have this daily maximum, and reached higher values in a parabolic fashion. The PAR observations were also parabolic because we had curated for particularly cloudy or rainy observations.

The sums of GPP and PAR from the mean diurnal cycles were stable and relatively insensitive to date range, and we used the four-week date range to best represent the typical midsummer climatology for the study area (Table 3). Deciduous trees consistently had the lowest GPP, and evergreen trees and turf grass had similar GPP, with turf grass being slightly greater than evergreen trees. Golf grass had by far the highest GPP, with estimates twice as large as turf grass. The PAR observations were very similar across all time periods with values approximately 12 MJ m^{-2} d^{-1}.

We divided the summed mean diurnal cycle of GPP by the product of the summed mean diurnal cycle of PAR and the FPAR at the in situ site to estimate an empirical LUE for each respective vegetation type: deciduous trees, evergreen trees, turf grass, and golf grass

(Table 4). We found that LUE was lowest for deciduous trees (0.24 gC MJ^{-1}) and highest for golf grass (1.14 gC MJ^{-1}), with evergreen trees (0.56 gC MJ^{-1}) and turf grass (0.66 gC MJ^{-1}) in between.

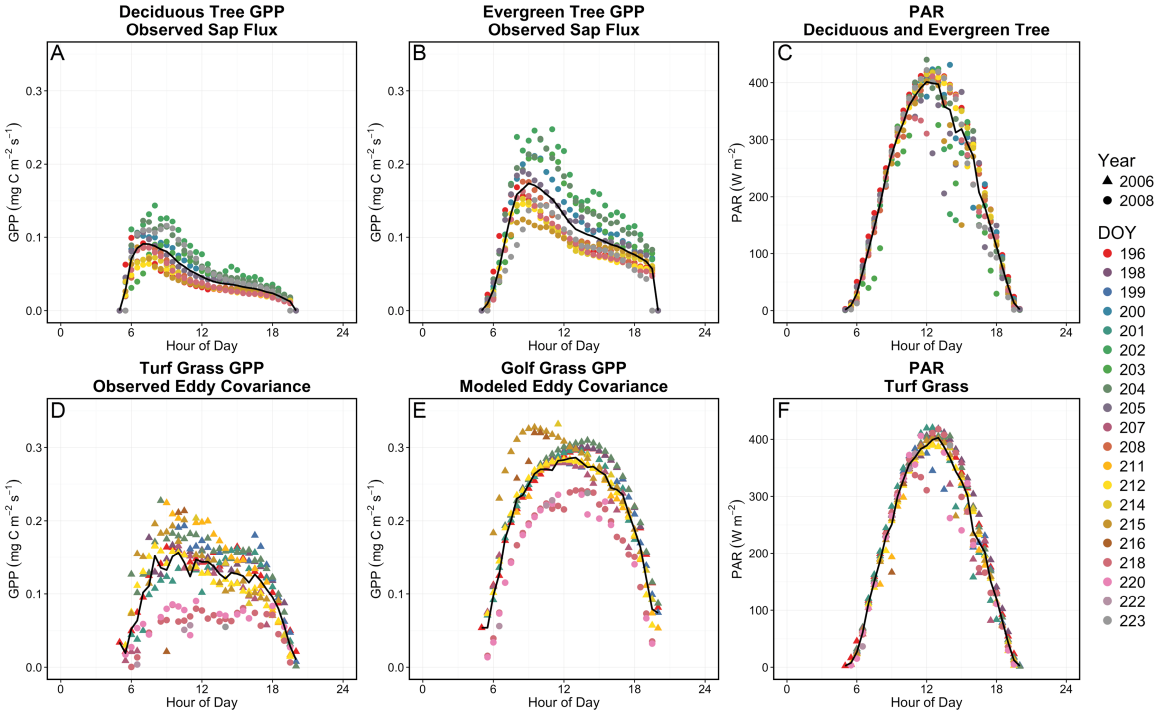

Figure 3: In situ flux observations used to calculate mean daily sums of GPP and PAR during 4-week window. Mean values at half hourly intervals are black lines, colors are day of year (DOY), triangles represent 2006 and circles 2008. The deciduous (A) and evergreen tree (B) GPP data were from sap flux measurements in 2008, the turf grass (D) GPP data were from eddy covariance measurements in 2006 and 2008, and the golf grass (E) GPP data were modeled based on turf grass eddy covariance measurements under peak growing conditions in 2006 and 2008. The PAR data for all vegetation types (C & F) were measured at the turf grass site from shortwave radiometer measurements multiplied by 0.45. Golf grass PAR (not shown) was assumed to be similar to turf grass PAR.

Table 3: Sum of mean diurnal cycles from in situ data of GPP (gC m^{-2} d^{-1}) and PAR (MJ m^{-2} d^{-1}) observations for 2-week (DOY 203-216), 3-week (DOY 199-219), and 4-week (DOY 196-223) intervals centered on July 28 (DOY 209). The 4-week interval values were used to calculate GPP across the study area. Data from the 40 m tower were missing for the 2-week interval because there were insufficient data to create a mean daily sum.

		2-week	3-week	4-week
GPP	Deciduous Tree	2.37	2.53	2.54
	Evergreen Tree	5.50	5.75	5.57
	Turf Grass	6.54	6.04	5.96
	Golf Grass	12.39	11.82	11.79
	40 m tower	NA	8.10	8.01
PAR	All Tree	11.99	11.94	12.08
	Turf Grass	12.01	11.99	12.15
	Golf Grass	11.95	11.95	12.11
	40 m tower	NA	12.08	12.09

Table 4: Parameters from sums of mean diurnal cycles and site polygons in FPAR image to estimate LUE: GPP (gC m^{-2} d^{-1}), PAR (MJ m^{-2} d^{-1}), FPAR (unitless), and LUE (gC MJ^{-1}).

	GPP	PAR	FPAR	LUE
Deciduous Tree	2.54	12.08	0.88	0.24
Evergreen Tree	5.57	12.08	0.83	0.56
Turf Grass	5.96	12.14	0.74	0.66
Golf Grass	11.79	12.11	0.86	1.14

D. Comparison to Tall Tower Flux Measurements

We used eddy covariance data from the 40 m tall KUOM tower to independently validate our GPP map. We used all available high quality observations during daylight (PAR > 0.45 W m^{-2}) during the same time periods in 2008 as were used for the in situ sites, and generated mean diurnal cycles of GPP and PAR from these data (Figure 4; Table 3). The GPP data at the flux tower exhibited a similar pattern to the turf site, but with a higher constant daily maximum value that was attained closer to noon than at the turf site. The PAR observations were similar to the observations for the other vegetation measurements in situ.

The summed mean diurnal cycles of GPP and PAR for the tall tower during the 4-week time period were 8.01 gC m^{-2} d^{-1} and 12.09 MJ m^{-2} d^{-1}, respectively, and we used this PAR value to calculate our GPP map based on the LUE model. We used 80% contribution polygons from the time points of the observations used to generate the mean diurnal cycle for the tower to delineate an area of comparison between our GPP map and the tall tower data (Figure 5). Our GPP map had a mean value of 7.10 gC m^{-2} d^{-1} for the parameterized vegetation classes within the comparison region, and had we not parameterized golf grass separate from turf grass, we would have obtained an estimate of only 5.09 gC m^{-2} d^{-1}. We considered our GPP map's estimate, which was 11% lower than the tower GPP, to be reasonable given the inherent variability in both our model and the tall tower's data.

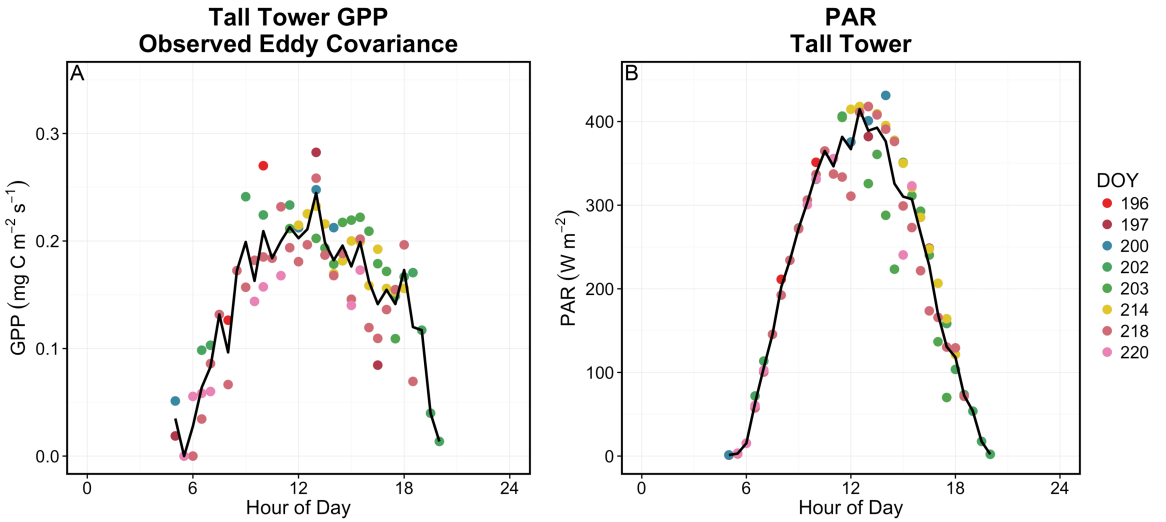

Figure 4: Observations used to generate summed mean diurnal cycles of GPP from eddy covariance (A) and PAR (shortwave radiometer * 0.45) (B) flux measurements from 40 m height on KUOM tower. Mean values at half hourly intervals are black lines and colors are day of year (DOY). All data are from 2008.

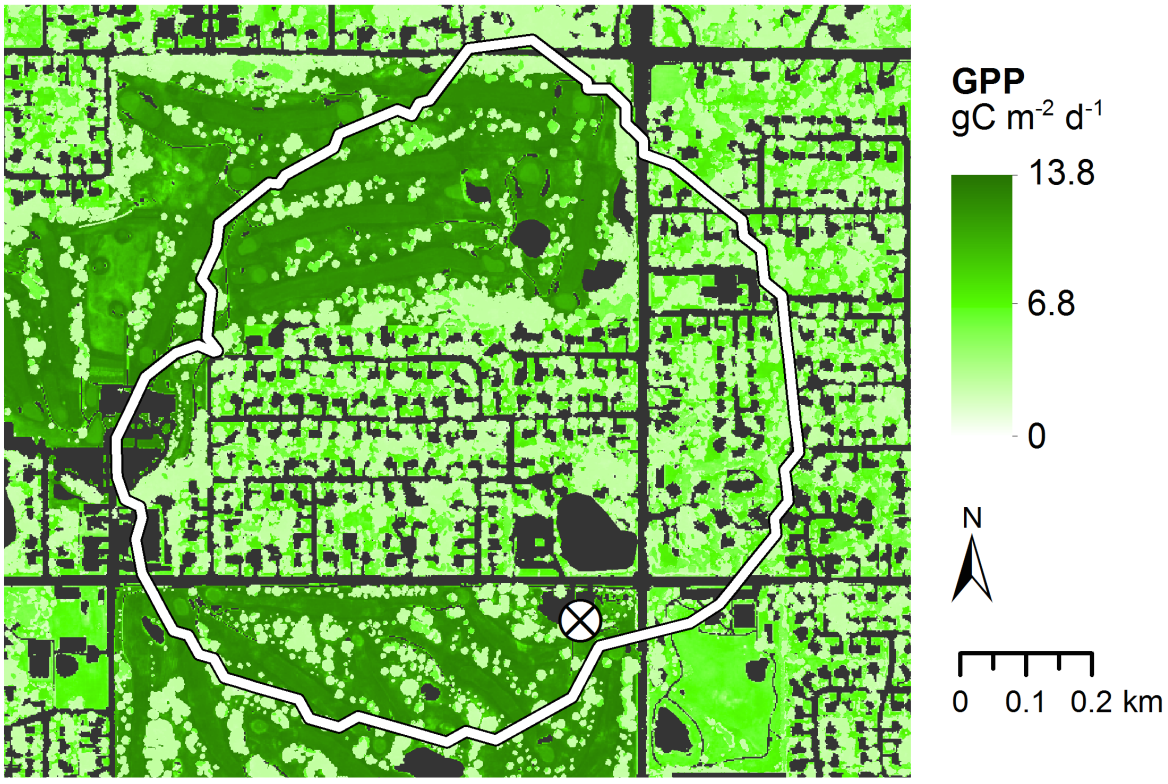

Figure 5: Union of high quality 80% contribution polygons forming tall tower ground footprint (white boundary, tower is 'X') during 4-week interval over a clipped out area of the GPP map. Non-vegetated areas are shown in black.

E. GPP Totals

We used the pixel-based GPP map to estimate typical daily GPP totals for regions in our study area (Table 5). We found that the majority of the vegetated area of the map consisted of deciduous trees and turf grass, with only small contributions from the evergreen trees and golf grass. For the total study area, the mean GPP across the parameterized vegetation classes and the impervious and soil class was 2.64 gC m^{-2} d^{-1}, and was 4.45 gC m^{-2} d^{-1} within the vegetation classes alone. The mean estimates of GPP were largely constant within vegetated classes across the selected regions. Deciduous trees had the lowest mean GPP (2.5 gC m^{-2} d^{-1}), and evergreen trees (5.8 gC m^{-2} d^{-1}) and turf grass (6.0 gC m^{-2} d^{-1}) had similar means, while golf grass (11.8 gC m^{-2} d^{-1}) had the highest mean GPP.

The contributions to total GPP by vegetation class were consistent across the selected regions, with turf grass contributing 55-60% and deciduous trees contributing 30% of the total GPP. Both classes had similar coverage in the study region, but the lower LUE of the deciduous trees resulted in lower GPP contributions overall. Evergreen trees and golf grass did not have large impacts on the GPP totals due to their small coverage area.

Table 5: Summary of vegetation classes and GPP within the full extent of the study area, the cities of Minneapolis and Saint Paul, and Ramsey County. (A) Total area (km^2); (B) Mean GPP ($gC\ m^{-2}\ d^{-1}$); (C) Total daily GPP ($Mg\ C\ d^{-1}$); and (D) Total daily GPP in percentages by vegetation type.

A. Areas (km^2)

	Full Study Extent	Minneapolis	Saint Paul	Ramsey County
Deciduous Tree	228.1	35.3	38.0	115.9
Evergreen Tree	22.3	2.1	3.3	13.5
Turf Grass	204.4	30.0	28.0	95.8
Golf Grass	11.1	1.3	1.7	4.9
Impervious and Soil	317.6	70.6	61.9	139.7
Total Vegetated	465.9	68.7	71.1	230.1
Total Area	894.0	148.6	145.0	439.8

B. Mean GPP ($gC\ m^{-2}\ d^{-1}$)

	Full Study Extent	Minneapolis	Saint Paul	Ramsey County
Deciduous Tree	2.52	2.45	2.51	2.54
Evergreen Tree	5.81	5.73	5.86	5.81
Turf Grass	6.05	5.97	6.02	6.10
Golf Grass	11.77	11.65	11.80	11.76
Total Vegetated	4.45	4.26	4.27	4.41
Total Vegetated + Impervious and Soil	2.64	2.10	2.28	2.75

C. Total GPP (Metric Tons)

	Full Study Extent	Minneapolis	Saint Paul	Ramsey County
Deciduous Tree	576	86	95	295
Evergreen Tree	129	12	19	78
Turf Grass	1236	179	169	584
Golf Grass	131	15	20	58
Total	2071	292	304	1015

D. GPP (%)

	Full Study Extent	Minneapolis	Saint Paul	Ramsey County
Deciduous Tree	27.8	29.5	31.4	29.0
Evergreen Tree	6.3	4.1	6.4	7.7
Turf Grass	59.7	61.2	55.5	57.6
Golf Grass	6.3	5.1	6.7	5.7

F. Variability of GPP Among and Within Vegetation Types

We derived estimates of GPP for each of the cover types, and calculated the mean, median, standard deviation (SD), and coefficient of variation (CV = SD / mean) (Table 6). All of the distributions were left skewed (Figure 6), but the CV for the turf grass was nearly twice as large as the CV for the other vegetation classes. Deciduous trees had a more peaked distribution and lower SD than the other classes, but a similar CV to evergreen trees and golf grass due to its lower mean GPP.

Table 6: GPP (gC m^{-2} d^{-1}) statistics for each vegetation cover type over the entire study area. CV is unitless.

	Mean	Median	SD	CV
Deciduous Tree	2.52	2.60	0.25	0.10
Evergreen Tree	5.81	5.92	0.52	0.09
Turf Grass	6.05	6.26	1.07	0.18
Golf Grass	11.77	12.10	1.20	0.10

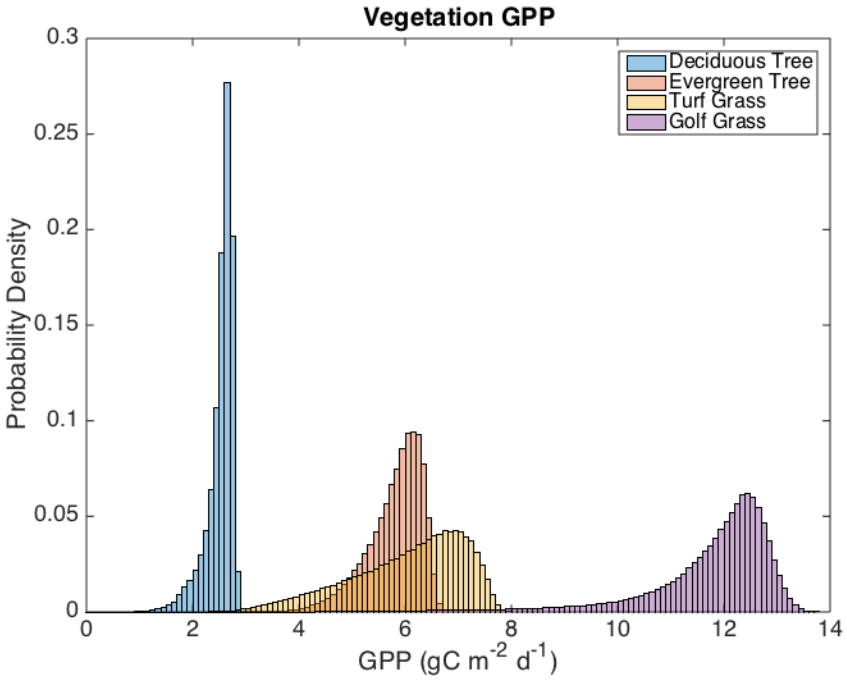

Figure 6: Normalized histogram of GPP (gC m^{-2} d^{-1}) for each vegetation cover type from entire study area.

G. GPP Among and Within Land Use Types

The percent cover of the vegetation classes varied widely by land use category (Table 7). We calculated percent cover from the vegetation classes and the impervious and soil class. We did not include the other land cover classes (water, wetlands, agriculture, and clouds / cloud shadows) in our percentage calculations because these were not typical built-up and urban vegetated land cover classes that were the focus of our GPP analysis.

Residential areas had 63.2% vegetation cover, with high proportions of deciduous trees (34.9%) and typical proportions of turf grass (24.9%) compared to the other land use categories. Deciduous trees had less than 10% cover in the most developed land use categories such as industrial, mixed use, retail, and airport, and much larger percentages in less developed areas, with high values of 46.7% cover in the park, recreational, or preserve class and 40.9% for undeveloped. Evergreen trees had marginal percent cover across all land use categories, with a maximum of 4.4% for the park, recreational, or preserve class. Turf grass had 26.1% cover for the total study area, and had the highest proportion of cover at 48.5% for the airport class. Golf courses were an extreme case with 65.3% grass cover and a total of 91.1% vegetation cover, even higher than parks, recreational, or preserves (85.7%). In general, as we compared land-use types from high to low total vegetation cover, losses of vegetation cover tended to come initially at the expense of deciduous tree cover, and later at the expense of turf grass after high levels (~70%) of impervious cover were reached.

Table 7: Percent cover within built-up and urban vegetation areas only, with other land cover classes removed (water, clouds, wetlands, and agriculture). Golf grass includes all turf grass within the golf course land use type. Darker shading indicates larger values.

	Impervious and Soil	All Vegetation	Deciduous Tree	Evergreen Tree	Turf Grass	Golf Grass
Total Study Area	40.5	59.5	29.1	2.8	26.1	1.4
Airport	47.1	52.9	3.9	0.5	48.5	0.0
Golf Course	8.9	91.1	21.8	4.0	0.0	65.3
Industrial	74.5	25.5	8.1	0.7	16.6	0.0
Institutional	50.3	49.7	16.0	1.6	32.1	0.0
Major Highway	56.7	43.3	7.3	0.5	35.4	0.0
Mixed Use	66.5	33.5	7.3	0.6	25.7	0.0
Office	71.5	28.5	10.5	0.8	17.1	0.0
Park, Rec., or Preserve	14.3	85.7	46.7	4.4	34.6	0.0
Residential	36.8	63.2	34.9	3.4	24.9	0.0
Retail	82.6	17.4	6.7	0.4	10.4	0.0
Undeveloped	15.6	84.4	40.9	4.0	39.5	0.0

Table 8: Mean GPP (gC m^{-2} d^{-1}) for the total study area by land use type for different land cover and vegetation type categories. The total area (km^2) of the class and the total daily GPP (Mg d^{-1}) are also included. Darker shading indicates larger values.

	Mean GPP (gC m^{-2} d^{-1})							
	All Veg. + Imp. and Soil	All Vegetation	Deciduous Tree	Evergreen Tree	Turf Grass	Golf Grass	Total Area (km^2)	Total GPP (Mg d^{-1})
Total Study Area	2.64	4.45	2.52	5.81	6.05	11.77	894	2071
Airport	2.57	4.85	2.58	6.12	5.02	0.00	11	27
Golf Course	8.48	9.31	2.59	5.89	0.00	11.77	18	151
Industrial	1.19	4.68	2.44	5.77	5.73	0.00	60	72
Institutional	2.40	4.82	2.48	5.64	5.95	0.00	54	129
Major Highway	2.17	5.01	2.46	5.67	5.52	0.00	37	80
Mixed Use	1.69	5.04	2.40	5.58	5.78	0.00	12	19
Office	1.32	4.63	2.41	5.63	5.94	0.00	10	13
Park, Rec., or Preserve	3.64	4.25	2.60	5.98	6.26	0.00	103	374
Residential	2.61	4.12	2.50	5.76	6.17	0.00	424	1106
Retail	0.76	4.38	2.37	5.60	5.63	0.00	40	31
Undeveloped	3.68	4.37	2.60	5.98	6.02	0.00	57	209

The variation in mean GPP by land use class was most pronounced when the area of impervious and soil was included (Table 8). Mean GPP within only vegetated pixels exhibited some variability, but was relatively modest, with differences mostly attributable to changes in the percentages of deciduous tree and turf grass cover. Golf courses were a notable exception, and with high vegetation cover did not experience a large difference with the inclusion of the impervious and soil class in the averaging. Turf grass accounted for the majority (59.0% – 94.8%) of the total GPP within each land use type (Table 9).

Mean values within unique vegetation classes tended to be largely similar across the different land use types, but did have some slight variation. The GPP by land use category varied within the vegetation classes themselves as well. Turf grass had the lowest mean GPP value in airports, while having the greatest values in the park, recreational, or preserve class and residential areas. Turf grass GPP in general had a much larger CV across the land use types than either of the tree classes (Table 10). The CV for golf grass GPP was similar to the tree classes rather than the turf grass in the majority of the study area. Deciduous trees had largely similar GPP estimates across land uses, but had lower values for the land use classes with greater than 50% impervious and soil cover than the other classes, with the lowest GPP estimates in the retail class. The CV of deciduous tree GPP tended to be larger in these less vegetated classes as well. Evergreen trees showed similar trends to the deciduous trees, with lower GPP values in the more impervious and soil covered classes, but with slightly less pronounced differences in CV.

Table 9: Percent contribution to total GPP of each parameterized vegetation class within each land use. Darker shading indicates larger values.

	Deciduous Tree	Evergreen Tree	Turf Grass	Golf Grass
Total Study Area	27.8	6.3	59.7	6.3
Airport	3.9	1.3	94.8	0.0
Golf Course	6.7	2.8	0.0	90.6
Industrial	16.5	3.6	79.9	0.0
Institutional	16.6	3.8	79.6	0.0
Major Highway	8.3	1.4	90.3	0.0
Mixed Use	10.3	1.9	87.7	0.0
Office	19.2	3.6	77.3	0.0
Park, Rec., or Preserve	33.3	7.2	59.6	0.0
Residential	33.5	7.5	59.0	0.0
Retail	20.7	2.9	76.4	0.0
Undeveloped	28.9	6.5	64.6	0.0

Table 10: Coefficient of variation for the total study area and major land use categories. Darker shading indicates larger values.

	Deciduous Tree	Evergreen Tree	Turf Grass	Golf Grass
Total Study Area	0.10	0.09	0.18	0.10
Airport	0.08	0.07	0.21	NA
Golf Course	0.07	0.08	NA	0.10
Industrial	0.12	0.10	0.20	NA
Institutional	0.11	0.10	0.17	NA
Major Highway	0.12	0.11	0.20	NA
Mixed Use	0.13	0.11	0.17	NA
Office	0.12	0.10	0.18	NA
Park, Rec., or Preserve	0.07	0.07	0.16	NA
Residential	0.10	0.09	0.16	NA
Retail	0.14	0.11	0.20	NA
Undeveloped	0.07	0.07	0.19	NA

Mean GPP had a strong linear relationship ($R^2 = 0.98$) with percent vegetation cover for all land use categories with the exception of golf courses (Figure 7A). Golf courses had the highest percent vegetation cover of all land use types, and the uniquely high LUE parameterization for golf grass resulted in a mean GPP twice as large as the prediction based on the linear trend from the other classes. Despite the variation in deciduous tree and turf grass percent cover and differences in LUE between the classes, the percent vegetation cover was strongly related to the differences in GPP between the land use categories. This is likely due to the tendency towards initial loss of deciduous tree cover and later turf grass as vegetation cover is reduced. Relationships between mean land use GPP and the percent cover of turf grass, deciduous trees, and evergreen trees (Figure 7) individually were still visibly linear, but were not as strong as the relationship with percent vegetation cover.

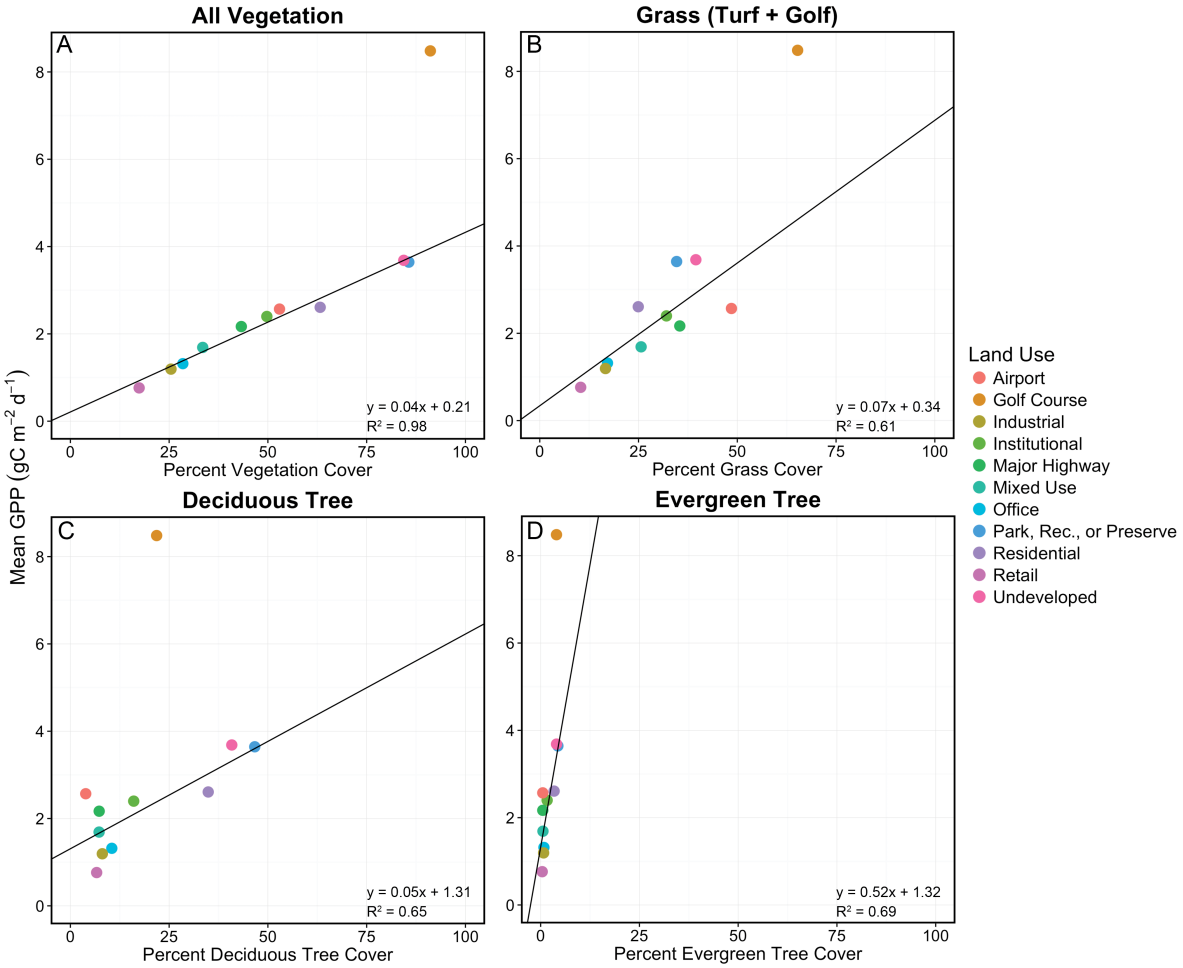

Figure 7: Mean GPP (all vegetation + impervious and soil, gC m^{-2} d^{-1}) of major land use types versus (A) percent vegetation cover, (B) percent grass (turf + golf) cover, (C) percent deciduous tree cover, and (D) percent evergreen tree cover. Golf courses have not been included in the linear regressions due to their unique parameterization for turf grass.

IV. Discussion

A. Evaluation of Urban GPP

1. Vegetation Cover and GPP Totals

Our GPP estimates were based on mean diurnal composites of GPP and incident PAR, and were not intended to represent the actual GPP for any single real day, but rather to represent typical GPP values during the midsummer period matching our WV-2 imagery (late July to early August). Based on our analysis, the GPP of our total study area of 894 km^2 was 2071 Mg C d^{-1} (Table 5). Percent vegetation cover was 52.1 % for the full study area, which is similar to vegetated, suburban regions in metropolitan Montreal, Canada (50%) (Bergeron and Strachan, 2011), Helsinki, Finland (44%) (Järvi et al, 2012), Syracuse, New York (48.2%) (Myeong et al., 2001), and a park site in Essen, Germany (52%) (Kordowski and Kuttler, 2010), but greater than other studies of dense urban regions (Nordbo et al., 2012). Total tree canopy cover was 28.0% for the full study area, similar with other studies using high spatial resolution imagery in Boston, Massachusetts (25.5%) (Raciti et al., 2014), downtown Santa Barbara, California (25.4%) (Alonzo et al., 2016), Syracuse, New York (26.6%) (Myeong et al., 2001) and Leipzig, Germany (19%) (Strohbach and Haase, 2012). Minneapolis and Saint Paul had similar total vegetated land areas, which resulted in similar estimates of total GPP for each city. However, Saint Paul had slightly higher mean GPP for each vegetation type, resulting in 0.18 gC m^{-2} d^{-1} more GPP on average (including impervious and soil) than Minneapolis. Ramsey County and the total study area had even greater mean GPP due to the increased mean GPP of both deciduous

trees and turf grass, whereas small differences in the mean GPP of evergreen trees and golf grass did not strongly affect the totals. Combined, those two classes never constituted greater than 14% of the total GPP for the full study area, Minneapolis, Saint Paul, or Ramsey County. While the evergreen tree and golf grass vegetation classes were widely scattered throughout the region, they were not the dominant factors driving urban GPP. Rather, turf grass was responsible for the more than half of the total GPP for the region due to its large area of coverage and relatively high mean GPP. Deciduous trees had the second largest area of coverage among vegetation classes, but had a lower mean GPP than the other vegetation classes, which led to it being responsible for only 27-32% of the total GPP for the selected regions. These percent contributions were remarkably constant across Minneapolis, Saint Paul, and Ramsey County, suggesting that there were not large differences in vegetation type composition or vegetation condition (as evidenced by FPAR) at the large scale of the major city or county spatial units.

Considering the patterns of GPP by land use class, residential areas covered nearly 50% of the total area in our study region, and they accounted for the largest share of the region's total GPP of all land use classes (Table 8). More heavily vegetated land use classes, namely parks, recreational areas, or preserves; undeveloped lands; and golf courses, had higher mean GPP, but they covered a smaller land area compared to residential land use. Residential areas had the highest GPP of the more developed urban land use types, mainly because they had more vegetation cover and higher mean GPP within the turf grass class. The higher turf grass GPP in residential areas may have been due to more intensive management including fertilizer application and irrigation (Milesi et al., 2005), and turf grass within the park, recreational, or preserve land use exhibited a similarly higher mean

GPP within turf grass covered areas. Overall, turf grass had a much larger CV than the other vegetation classes, likely due to this variability in maintenance.

Our study region's mean GPP (2.64 gC m^{-2} d^{-1}) was much lower than GPP reported for the Detroit metropolitan region by Zhao et al. (2007), which was nearly 15 gC m^{-2} d^{-1} on average. This is partially attributable to differences in light use efficiency parameters, which in Zhao et al.'s (2007) study were based on natural forests, grasslands, and agricultural crops (Turner et al., 2003b) and scaled by typical fractional vegetation cover estimates within AVHRR pixels based on Landsat-derived land cover. Another major factor was the increased extent of their study region far beyond the core urban region of the city (Zhao et al., 2007), which could lead to distinct differences in vegetation function becoming dominated by non-urban tree cover.

The mean of our mapped estimate of vegetation GPP within the tower footprint was 11% lower than the GPP observations by the tall tower. We considered this difference to be reasonable given multiple sources of error in the flux to map comparison. First, the land cover map is subject to error in classification, and thus parameterization of GPP by vegetation class. Relative error in the tree GPP sap flux was assumed to be 29% and 23% for evergreen and deciduous trees, respectively (Peters and McFadden, 2012). Second, inherent to the eddy covariance technique are errors associated with bias due to sensor configuration and data processing of typically 5–10%, and also random errors due to atmospheric turbulence of ~5% (Baldocchi, 2008). There are also errors in removing anthropogenic fluxes at our site (Menzer et al., 2015). Lastly, there are errors associated with the modeling of the flux footprint including changes in wind direction, the threshold of 80% of the flux

attribution, and our measurements occurring a non-homogeneous surface (Kljun et al., 2004).

2. FPAR

We used a linear NDVI-FPAR relationship from Sims et al. (2006a) for all of our vegetation classes. The relationship between NDVI and FPAR has been shown to be near-linear for many types of vegetation (Ruimy et al., 1994; Myneni and Williams, 1994; Song et al., 2013). The relationship in Sims et al. (2006a) has been used in other studies based on MODIS NDVI (e.g. Wu et al., 2012; Zhang et al., 2016). FPAR has also been estimated in the remote sensing literature using relationships with other spectral indices such as the Enhanced Vegetation Index (EVI) (e.g. Sims et al., 2006b; Mahadevan et al., 2008) and radiative transfer models (e.g. Knyazikhin et al., 1999; Myneni et al., 2002).

The FPAR of the grass at our turf site derived from the WV-2 image was 0.74. This reflects the summer dormancy typical of C3 turf grasses in the region compared with the more uniformly irrigated and well-maintained golf grass's mean FPAR (0.86). We found that the relationship in Wu and Bauer (2012) would have resulted in a lower FPAR estimate. The authors' NDVI-FPAR relationship (FPAR = 1.29 * NDVI – 0.29) was measured in the field on lawns near our turf site, but had a lower offset and greater slope than the relationship we used from Sims et al. (2006a). Our estimates for FPAR for turf grass are similar to midsummer values of ~0.7 for a corn and soybean site in Illinois (Turner et al., 2005; Meyers and Hollinger, 2004) and a value of ~0.8 for a tallgrass prairie site in eastern Kansas (Turner et al., 2006; Ham and Knapp, 1998).

Our deciduous tree and evergreen tree FPAR estimates correspond well with estimates in Turner et al. (2005) for the respective vegetation types (Wofsy et al., 1993;

Anthoni et al., 2002) and to mixed forest in Turner et al. (2006) (Davis et al., 2003). In general, trees did not show a large amount of variability in FPAR in comparison to the turf grass, and this may be due to the lack of summer dormancy in trees (Peters and McFadden, 2012; Turner et al., 2005). The FPAR at the sap flux sites was lower than the median overall, but not atypical for open-grown trees in park-like conditions with a variety of canopy densities. More tightly grown trees in the forested regions of our study area tended to have higher FPAR values.

3. Light Use Efficiency

In this study, we calculated an empirical LUE value for each urban vegetation type using daily GPP and PAR totals from in situ measurements in combination FPAR estimates from WV-2 NDVI. The empirical LUE values we derived were applied as constants across our study area. Often, global models of GPP group similar biomes and plant functional types into single classes, resulting in only a few different vegetation classes overall at the global scale (e.g. Prince and Goward, 1995). A maximum LUE is derived for each of these vegetation classes, either from field data, remote sensing, or modeling, and the maximum value is then attenuated on a per-pixel basis by scaling based on environmental variables such as temperature and vapor pressure deficit (VPD) (e.g. Heinsch et al., 2003). The scalars attempt to account for seasonality and variability between distinct biomes with broadly similar plant functional types. Since the empirical LUE values we have derived here are locally parameterized, we did not need to modify our LUE values by environmental conditions due to broad similarities in conditions across the study area. While LUE likely varies spatially at highly local scales by species, shading, soil, and other factors (Ahl et al., 2004; Schwalm et al., 2006), our LUE values were representative of average values for the

majority of vegetation. However, our empirical LUE values are only representative of clear, midsummer days in our study area, and are not indicative of LUE for all seasons and solar radiation conditions. While we have in situ flux measurements available on a daily basis for multiple years, to properly characterize the annual cycle of LUE with our techniques would require a corresponding time series of high resolution imagery (e.g., WV-2), which is unavailable. In the future, if at least a few seasonal time points are available in high resolution imagery, it may be feasible to use data fusion techniques with daily imagery such as MODIS (e.g., Gao et al., 2006, Kim and Hogue, 2012) to a complete seasonal time series of high resolution FPAR estimates.

We compared our empirical LUE estimates to estimates of LUE based on the Daily GPP and Annual NPP (MOD17A2/A3) Products User's Guide Version 3.0 (Running and Zhao, 2015; Yang et al., 2007). MOD17 GPP has maximum LUE values for various vegetation classes that are scaled down by linear ramp functions related to minimum daily temperature and VPD based on gridded meteorological data. To estimate MOD17 LUE for our study area, we used temperature and VPD data from our in situ turf site with the half hourly time points that we had used to calculate our empirical turf grass LUE. The MOD17 LUE estimates were not affected by minimum air temperature because the minimum air temperature (~17.0° C) during this interval was larger than the upper temperature threshold for LUE scaling for all MOD17 vegetation classes. However, the MOD17 LUE for each class was affected by VPD, and we calculated mean daily VPD estimates based on both the mean (2.018 kPa) and the median (1.881 kPa) at each half hourly time point (Figure 8).

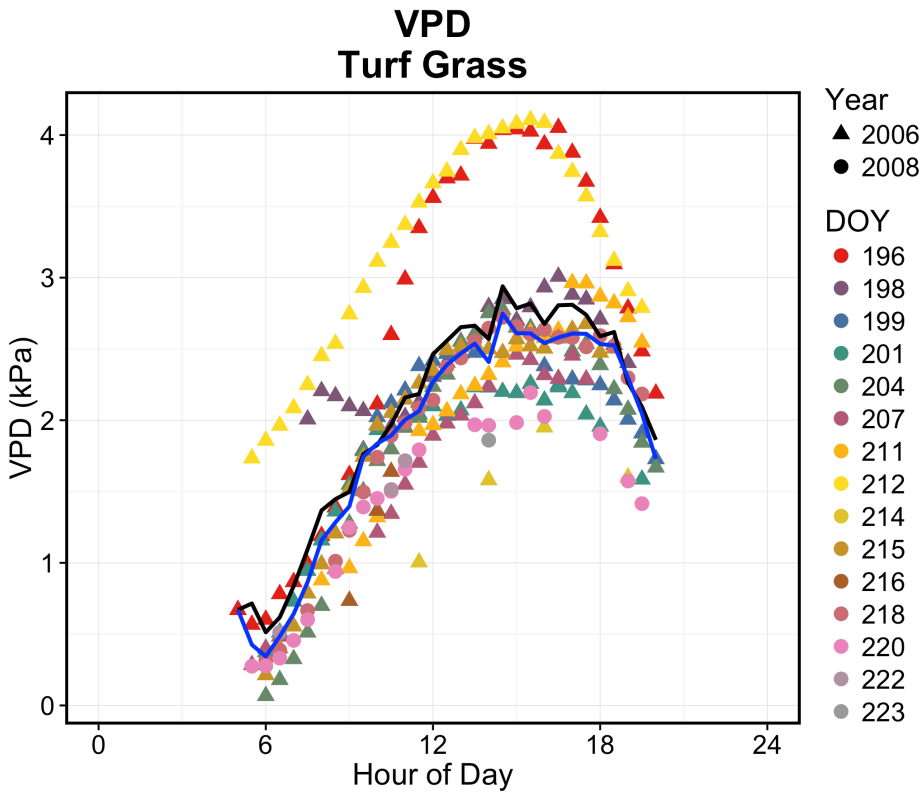

Figure 8: Typical mean daily VPD estimates derived from half hourly observations at the turf grass flux tower site. The half hourly means are indicated by the black line (mean = 2.018 kPa), and the half hourly medians by the blue line (mean = 1.881 kPa).

Table 11: Comparison between our empirical LUE estimates and estimates for scaled MODIS GPP (MOD17) LUE by vegetation class. LUE estimates are gC MJ^{-1}.

This Study		Estimated MODIS GPP (MOD17)		
Vegetation Class	LUE	Vegetation Class	LUE (VPD = 2.018 kPa)	LUE (VPD = 1.881 kPa)
Deciduous Tree	0.24	Evergreen Needleleaf Forest	0.63	0.66
Evergreen Tree	0.56	Evergreen Broadleaf Forest	0.60	0.67
		Deciduous Needleleaf Forest	0.19	0.28
		Deciduous Broadleaf Forest	0.00	0.00
		Mixed Forest	0.23	0.31
		Closed Shrubland	0.85	0.89
		Open Shrubland	0.56	0.59
		Woody Savanna	0.57	0.64
Turf Grass	0.66	Savanna	0.53	0.60
Golf Grass	1.14	Grassland	0.61	0.63
		Cropland	0.65	0.69

With the exception of golf grass, our empirical LUE estimates generally corresponded well with the MOD17 LUE estimates (Table 11). Our deciduous tree LUE (0.24 gC MJ^{-1}) is similar to the MOD17 mixed forest LUE (0.23 and 0.31 gC MJ^{-1}), but the MOD17 deciduous broadleaf forest LUE had been scaled to 0 gC MJ^{-1} due to the high VPD observations. Our evergreen tree LUE (0.56 gC MJ^{-1}) is similar to the MOD17 evergreen needleleaf forest LUE (0.63 and 0.66 gC MJ^{-1}), and our turf grass LUE (0.66 gC MJ^{-1}) is similar to the MOD17 LUE estimates for the herbaceous classes of savanna (0.53 and 0.60 gC MJ^{-1}), grassland (0.61 and 0.63 gC MJ^{-1}), and cropland (0.65 and 0.69 gC MJ^{-1}). Our golf grass LUE (1.14 gC MJ^{-1}) is much higher than any of the MOD17 LUE estimates for any vegetation class. We could have likely used MOD17 LUE estimates based on our in situ VPD observations for our evergreen tree and turf grass GPP calculations, but deciduous trees, without knowing a priori to substitute the MOD17 mixed forest class, and golf grass would not have had accurate GPP estimates with these parameters.

In addition, we compared our clear-sky, midsummer empirical LUE values to several example literature values for similar vegetation types (Table 12). Our golf grass LUE is high and our turf grass LUE is low compared to many literature estimates for grasslands. Both of our estimates were lower than maximum estimates for turf grass LUE at various levels of nitrogen application from Wu and Bauer (2012) when converted to GPP LUE from NPP LUE using a ratio of NPP/GPP = 0.5. Our evergreen and deciduous tree LUE estimates are both low compared to literature estimates. Although many studies indicate higher LUE for deciduous trees than for evergreen trees (Ruimy et al., 1994; Still et al., 2004), we found our evergreen tree LUE was twice that of our deciduous tree LUE. We refer to summaries in Ruimy et al. (1994) and Goetz and Prince (1999) for further LUE comparisons.

Table 12: Comparisons of our empirical LUE values to literature values. Literature LUE marked with '*' have been converted to GPP LUE from NPP LUE using a ratio of NPP/GPP = 0.5, and vegetation types denoted with 'max' are maximum LUE parameters that are normally adjusted downward by environmental scalars to estimate GPP.

This Study		Literature		
Vegetation Class	LUE	Vegetation Class	LUE	Reference
Turf Grass	0.66	Grassland (max)	0.86	Yang et al., 2007
Golf Grass	1.14	Cropland (max)	1.47	
		Desert Grassland	~0.5	
		Corn and Soybean (MODIS)	~0.5	Turner et al., 2005
		Corn and Soybean (BigFoot flux model)	~2.0	
		Tallgrass Prairie (MODIS)	~0.5	Turner et al., 2006
		Tallgrass Prairie (BigFoot flux model)	~1.5	
		Turf Grass (high N; max)	2.16*	
		Turf Grass (med. N; max)	1.68*	Wu and Bauer, 2012
		Turf Grass (low N; max)	1.3*	
Evergreen Tree	0.56	Boreal Forest	~1.0	Turner et al., 2005
		Dryland Needleleaf Forest	~0.5	
		Evergreen Needleleaf Forest (max)	1.02	Yang et al., 2007
Deciduous Tree	0.24	Deciduous Broadleaf Forest	~12	Turner et al., 2005
		Deciduous Broadleaf Forest (max)	1.56	Yang et al., 2007
		Mixed Forest	~1.0	Turner et al., 2006
		Mixed Forest (max)	1.31	Yang et al., 2007

B. Comparison to Natural Vegetation

Our mean GPP of 2.64 gC m^{-2} d^{-1} for the full study area (including the large fraction of non-vegetated impervious surfaces) is lower than GPP estimates for many natural ecosystems (Yuan et al., 2007). Compared in this way, GPP of the metropolitan region is more similar to desert grassland or tundra than to natural temperate broadleaf deciduous forest or tallgrass prairie (Turner et al., 2005). Due to similarities in urban land cover composition (McKinney, 2006), the GPP of the Minneapolis-Saint Paul metropolitan region likely has more in common with other midwestern cities such as Milwaukee and Chicago than the surrounding natural forests and grasslands. Additionally, the mean GPP of all vegetation (*excluding* impervious surfaces) in our full study area was 4.45 gC m^{-2} d^{-1}, which is much lower than the ~8 – 14 gC m^{-2} d^{-1} that is typical for nearby mixed forests (Lost Creek, Wisconsin, Davis et al., 2003; Sylvania, Wisconsin, Desai et al., 2005; UMBS, Michigan, Curtis et al., 2005), deciduous broadleaf forests (Willow Creek, Wisconsin, Bolstad et al., 2004) and grasslands (Walnut River, Kansas, Song et al., 2005) (Yuan et al., 2007), and is more similar to a boreal evergreen needleleaf forest site in Manitoba (Boreas NSA, Goulden et al., 2006) (Yuan et al., 2007).

Our turf site grass experienced peak uptake in May (Peters and McFadden, 2012), and the GPP estimates we make in this study were characteristic of the midsummer dormancy period typical of C3 grasses. The golf grass GPP was modeled based on the peak uptake for turf grass, assuming relatively little in the way of nutrient or water limitations. Although there is no direct comparison for turf grass in natural ecosystems, turf grass GPP can be compared to estimates for grasslands and herbaceous crops. Our turf grass GPP estimates were much lower than a tallgrass prairie site in Kansas (Walnut River, Song et al.,

2005), but were very similar to an abandoned agricultural field near Duke Forest in North Carolina (Duke Grass, Novick et al., 2004) (Yuan et al., 2007). Furthermore, our estimates for turf grass GPP were much larger than midsummer estimates for a desert grassland site in New Mexico (Sevilleta LTER, Kurc and Small, 2004), and much smaller than a corn and soybean site in Illinois (Meyers and Hollinger, 2004) as estimated from flux towers and MODIS GPP (Turner et al., 2005). Our golf grass GPP was more similar to the aforementioned tallgrass prairie and corn and soybean sites.

Our GPP estimates for deciduous trees were lower than many of the values reported in the literature for natural forests (e.g. Turner et al., 2003; Turner et al., 2005; Heinsch et al., 2006). Our estimates are local to our study area as they were trained on the in situ measurements based on sap flux from Peters and McFadden (2012). Reductions in GPP may be because open grown trees, typical of urban areas, tend to have less above ground biomass than trees with similar heights and DBH measurements in forests (Nowak, 1994). Urban trees experience many local environmental stresses (Oke, 1989) that likely impact GPP per unit area. On an annual scale, it is possible to expect increased carbon uptake in deciduous trees in urban areas due to an extended growing season from increased temperatures in the urban heat island (Keenan et al., 2014; Melaas et al., 2016), but reductions in growth may mitigate the benefits of such increases (Reinmann and Hutyra, 2017). Evergreen tree GPP in our study area was similar to estimates from flux measurements at a dryland temperate conifer forest site in Oregon (Anthoni et al., 2002) and a boreal forest site in northern Manitoba (Goulden et al., 1997) at the peak daily rate (Turner et al., 2005; Heinsch et al., 2006).

C. Variability Within Vegetation Types

In our mapped estimates, LUE and PAR were held constant across the study area, thus GPP variability within the vegetation classes was due to spatial variations in FPAR, which was derived from WV-2 NDVI. The GPP estimates for the tree and golf grass classes were more tightly clustered than the turf grass class, which had significantly higher variability than all of the other urban vegetation classes. The variations in FPAR, and thus GPP, within the turf grass class were most likely due to differences in the intensity of lawn management. This may have been even more clearly expressed because our imagery was from the midsummer period when C3 turf grasses experience a period of dormancy which can vary with site conditions such as solar exposure and management practices, especially irrigation. In contrast, trees do not experience midseason dormancy like the C3 turf grasses, and the golf grass can be expected to have a more uniformly high level of maintenance, with significant nutrient inputs through fertilizers and intensive irrigation to reduce the stress of midsummer high temperatures on the turf grass. The productivity of trees did not appear to vary strongly across our study area as evidenced by their low spatial variations in FPAR; however, this may have been be due to saturation of the NDVI at high levels of canopy density (Huete, 1988), potentially resulting in a ceiling for our GPP ranges in trees. These differences would likely be even more pronounced when distinguished by species (Peters and McFadden, 2012; Ahl et al., 2004).

At the citywide and regional scales, the distributions of turf grass GPP estimates were similar. The larger range of GPP in turf grass was likely attributable to the variety of management levels within the class (Wu and Bauer, 2012; Milesi et al., 2005). Some turf grasses are well maintained, and may in fact have similar GPP to golf grass, while other turf

grasses have low levels of maintenance, resulting in lower GPP estimates. These low GPP turf grasses may be pixels with larger percentages of bare soil, which would further reduce GPP estimates. Instead of using a strict threshold in NDVI, we distinguished the impervious and bare soil class from the vegetation using a maximum likelihood classifier, which we found gave us a better result for including senesced grasses in the turf grass class based on visual inspection. This classification technique contributes to the diversity of GPP values for grass, including lower GPP estimates than would otherwise be included based on thresholding.

D. Variability Among Land Use Types

Often, studies of urban GPP stratify by land use type or urban density classes and then assign vegetation classes and LUE parameters accordingly (e.g. Zhao et al., 2007). In this study we were able to resolve fine scale patterns of each major urban vegetation type within different land use units, and thus estimate contribution to GPP from the proportion of vegetation cover within each land use. The percent vegetation cover varied widely by land use type (Table 7), and a uniform percent cover for the study region would be inappropriate to apply due to the diversity of cover. However, varying percent vegetation cover within a Landsat or MODIS pixel to estimate GPP may be possible if the distribution of vegetation types relative to each other is uniform at a sufficient scale for analysis (Figure 7). At present, we are unable to make annual estimates of GPP for our full study region, but if strong relationships with reflectance estimates from MODIS exist, we could potentially scale our data across an annual cycle, with the caveat of being unable to distinguish the timing of green up and senescence of specific grass versus tree pixels in our scene.

The residential land use type represented more than half (1106 Mg d^{-1}) of the total daily GPP (2071 Mg d^{-1}) for the full study region due to its large area (424 km^2, 47% of the full study area) and relatively high mean GPP (2.61 gC m^{-2} d^{-1}) among the built-up and urban vegetation land cover classes (Table 8). Parks, recreational areas, or preserves and undeveloped areas also had relatively high contributions to the total. Interestingly, these two classes had the highest estimates of mean GPP for deciduous trees, and had among the highest mean GPP for grass, along with the residential class. This may imply that, in urban areas, vegetation might be more productive due to greater transpiration in areas with greater vegetation cover, perhaps as a result of lower temperatures and a lower vapor pressure deficit in more vegetated regions (Kjelgren and Montague, 1998). An alternative possibility is that the less vegetated areas had a greater proportion of pixels that were mixed with impervious surfaces, which would reduce the apparent GPP due to the effect of mixed pixels on NDVI (Wetherley et al., 2017). This effect should have been limited at high spatial resolution used in our study as compared to previous work on urban GPP that used coarser resolution imagery such as Landsat; however, even at the 2 m resolution of our imagery there undoubtedly were small effects due to edges or the presence of bare soil within turf grass lawns, for example.

Evaporative demand can be greater in urban vegetation near impervious surfaces as well due to advection. For example, Spronken-Smith et al. (2000) found that an irrigated urban park in Sacramento, California evaporated ~35% more water than a rural irrigated sod farm outside of the city. Without sufficient irrigation, urban C3 turf grasses are limited in their GPP at high levels of potential evapotranspiration and temperature (Peters and McFadden, 2012). Field experiments of well-watered plants have shown that isolated plants

surrounded by impervious surfaces tend to have much higher transpiration rates than less isolated plants (Hagishima et al., 2007). Increased tree GPP in more densely vegetated regions may also be related to differences in crown shape and growth patterns between forest and non-forest trees. Land use classes with more impervious surface cover had reduced mean GPP mainly due to their relative lack of vegetation, but the mean GPP by vegetation class within these land uses was also slightly reduced relative to the more vegetated land use types. The coefficient of variation by vegetation class did vary by land use type as well, but did not reflect any easily identifiable trend between land uses.

E. Implications for Urban Vegetation Carbon Budget

Characterization of urban GPP is important to improve understanding of the initial inputs and pathways of carbon in urban ecosystems, but high rates of GPP do not necessarily imply high rates of carbon uptake and storage via NPP (NPP = GPP – Plant Respiration). In our study area, turf grasses are likely to be net sources of atmospheric CO_2 during midsummer due to temperature-induced dormancy, resulting in high rates of respiration exceeding GPP (Peters and McFadden, 2012). At our turf grass site, Hiller et al. (2011) found that over the course of two years of study, the site was a net source in 2007 due to hot, dry summertime conditions, but was a net sink in 2008 under more typical weather (growing-season mean air temperatures were 15.2° C in 2007 and 13.2° C in 2008) (Peters and McFadden, 2012). Irrigated, recreational turf grasses such as golf courses were not as impacted by the high temperatures as were non-irrigated, residential turf grasses. In addition, while natural ecosystems such as tallgrass prairies can take up large amounts of carbon in soil organic matter over time, in urban turf grass, shallow rooting depth and maintenance

practices such as aerification tend to limit the amount of soil organic matter that can be stored. Although well-irrigated areas tend to produce greater initial sinks through greater biomass production (Milesi et al., 2005), areas of lower maintenance (e.g. certain residential areas) may produce greater sinks in soil over time than highly managed recreational areas (Pouyat et al., 2006).

Both deciduous and evergreen tree species at our sites were net sinks during 2007 and 2008 (Peters and McFadden (2012). Trees store carbon as wood (Nowak, 1994) in addition to producing soil organic matter, and have greater long term carbon storage with typical average NPP:GPP ratios of forests being ~0.5 with high variability (Waring et al., 1998; DeLucia et al., 2007). For example, net uptake has been shown to vary significantly with stand age in managed forests (Noormets et al., 2007). Furthermore, dense tree canopy cover (leaf area) may result in reduced CO_2 flux from soils due to local temperature reduction (Peters and McFadden, 2010). Although spatial modeling of plant respiration and thus NPP was beyond the scope of this study, we note that in our study area net carbon uptake over time was likely to be mainly driven by tree cover rather than turf grasses. Therefore, land use types with high proportions of tree cover (residential; park, recreational, or preserve; undeveloped) likely have the greatest effect on urban net carbon uptake.

The potential of future urban expansion makes it critically important to understand environmental effects within urban areas. Urban growth often replaces existing vegetation cover, and characterization of ecosystem services from vegetation, such as GPP, will become an increasingly necessary consideration for sustainable development. For residential homeowners in the Minneapolis-Saint Paul metropolitan area, although turf grass has high GPP, this does not imply high NPP, and trees are more likely avenues of long-term carbon

storage. Our study aims to contextualize urban GPP as part of global carbon cycle monitoring, with hopes of enhancing future urban planning strategies in regards to carbon uptake.

V. Conclusions

In this study, we analyzed variations in GPP across the 894 km^2 Minneapolis-Paul metropolitan region. First, we investigated the magnitude and variability of GPP within and among the major urban vegetation classes in the study area. Deciduous trees had the lowest mean GPP while golf grass had the highest, and the coefficient of variation for turf grass GPP was twice as large as for the other vegetation types. Second, we compared GPP within major urban land use types to determine whether land use GPP was more determined by the fractional cover of different vegetation types or by the rate of GPP within the vegetation types. Percent vegetation cover generally described differences in land use GPP. However, there were differences between land use types in mean GPP by vegetation class, with more vegetated land use types tending to have higher GPP estimates. Third, we compared our estimates of urban vegetation GPP to natural vegetation, and used our in situ data to suggest likely estimates of NPP. On a total area basis, urban GPP tended to be low relative to natural forests and grasslands due to reduced total vegetation cover. Excluding non-vegetated surfaces, mean urban vegetation GPP tended to be lower than comparable natural vegetation GPP, mainly due to the low GPP of deciduous trees.

It is important to note that these differences refer strictly to GPP, which was the focus of our study. When taking plant and soil respiration into account (i.e., NPP or net ecosystem exchange of CO_2), our in situ flux data show that, on an annual basis, turf grass in

our study area can be a net source or a sink of carbon, while trees were reliable sinks. Further work would use remote sensing data fusion techniques to evaluate seasonal changes in the spatial variability of GPP by vegetation and land use type, and would help to extrapolate our current results to an annual cycle. The present study showed that high spatial resolution imagery can reveal important patterns of variability in urban GPP compared to lower resolution sensors; however, the total percent vegetation cover provided reasonable estimates of GPP at large scales for the urban area. This suggests that urban GPP can be adequately quantified at the metropolitan scale using coarser resolution sensors and fractional vegetation cover estimates given that vegetation LUE is appropriately parameterized, but higher resolution imagery is necessary to compare within and among neighborhoods, land use types, and vegetation cover classes.

VI. References

Adler-Golden, S., Berk,A., Bernstein, L.S., Richtsmeier, S., Archarya, P.K., Matthews, M.W., Anderson, G.P., Allred, C.L., Jeong, L.S., and Chewynd, J.H., 1998, FLAASH, a MODTRAN4 Atmospheric Correction Package for Hyperspectral Data Retrievals and Simulations, Summaries of the 7th JL Airborne Earth Science Workshop, Vol. 1, 9-14.

Ahl, D. E., Gower, S. T., Mackay, D. S., Burrows, S. N., Norman, J. M., & Diak, G. R. (2004). Heterogeneity of light use efficiency in a northern Wisconsin forest: implications for modeling net primary production with remote sensing. *Remote Sensing of Environment*, *93*(1–2), 168–178.

Alonzo, M., Bookhagen, B., & Roberts, D. A. (2014). Urban tree species mapping using hyperspectral and lidar data fusion. *Remote Sensing of Environment*, *148*, 70–83. http://doi.org/10.1016/j.rse.2014.03.018

Alonzo, M., McFadden, J. P., Nowak, D. J., & Roberts, D. A. (2016). Mapping urban forest structure and function using hyperspectral imagery and lidar data. *Urban Forestry & Urban Greening*, *17*, 135–147. http://doi.org/10.1016/j.ufug.2016.04.003

Anthoni, P. M., Unsworth, M. H., Law, B. E., Irvine, J., Baldocchi, D. D., Tuyl, S. Van, & Moore, D. (2002). Seasonal differences in carbon and water vapor exchange in young and old-growth ponderosa pine ecosystems. *Agricultural and Forest Meteorology*, *111*(3), 203–222. http://doi.org/10.1016/S0168-1923(02)00021-7

As-syakur, A. R., Osawa, T., & Adnyana, I. W. S. (2010). Medium spatial resolution satellite imagery to estimate gross primary production in an urban area. *Remote Sensing*, *2*(6), 1496–1507. http://doi.org/10.3390/rs2061496

Baldocchi, D. D. (2008). "Breathing" of the terrestrial biosphere: lessons learned from a global network of carbon dioxide flux measurement systems. *Australian Journal of Botany*, *56*(15), 1–26. http://doi.org/doi:10.1071/BT07151

Bergeron, O., & Strachan, I. B. (2011). CO2 sources and sinks in urban and suburban areas of a northern mid-latitude city. *Atmospheric Environment*, *45*(8), 1564–1573.

Bolstad, P. V, Davis, K. J., Martin, J., Cook, B. D., & Wang, W. (2004). Component and whole-system respiration fluxes in northern deciduous forests. *Tree Physiology*, *24*(5), 493–504. http://doi.org/10.1093/treephys/24.5.493

Burian, S. J., & Pomeroy, C. A. (2010). Urban Impacts on the Water Cycle and Potential Green Infrastructure Implications. In: *Urban Ecosystem Ecology*, Agron. Monogr. 55. ASA, CSSA, SSSA, Madison, WI. 277-296. doi:10.2134/agronmonogr55.c14

Buyantuyev, A., & Wu, J. (2009). Urbanization alters spatiotemporal patterns of ecosystem primary production: A case study of the Phoenix metropolitan region, USA. *Journal of Arid Environments*, *73*(4–5), 512–520. http://doi.org/10.1016/j.jaridenv.2008.12.015

Cadenasso, M. L., Pickett, S. T. A., & Schwarz, K. (2007). Spatial heterogeneity in urban ecosystems: reconceptualizing land cover and a framework for classification. *Frontiers in Ecology and the Environment*, *5*(2), 80–88.

Chapin, F. S., III (1993). Functional role of growth forms in ecosystem and global processes. In J. Ehleringer & C. Field (Eds.), *Scaling physiological processes: leaf to globe* (pp. 287–312). San Diego: Academic Press.

Chapin, F. S., III, Matson, P. A., & Mooney, H. A. (2002). *Principles of Terrestrial Ecosystem Ecology*. New York, NY: Springer-Verlag.

Curtis, P. S., Vogel, C. S., Gough, C. M., Schmid, H. P., Su, H. B., & Bovard, B. D. (2005). Respiratory carbon losses and the carbon-use efficiency of a northern hardwood forest, 1999-2003. *New Phytologist*, *167*(2), 437–455.

D'Odorico, P., Gonsamo, A., Pinty, B., Gobron, N., Coops, N., Mendez, E., & Schaepman, M. E. (2014). Intercomparison of fraction of absorbed photosynthetically active radiation products derived from satellite data over Europe. *Remote Sensing of Environment*, *142*, 141–154. http://doi.org/10.1016/j.rse.2013.12.005

Davis, K. J., Bakwin, P. S., Yi, C., Berger, B. W., Zhao, C., Teclaw, R. M., & Isebrands, J. G. (2003). The annual cycles of CO2 and H2O exchange over a northern mixed forest as observed from a very tall tower. *Global Change Biology*, *9*, 1278–1293. http://doi.org/10.1029/2009JD012832

DeLucia, E. H., Drake, J. E., Thomas, R. B., & Gonzalez-Meler, M. (2007). Forest carbon use efficiency: Is respiration a constant fraction of gross primary production? *Global Change Biology*, *13*(6), 1157–1167. http://doi.org/10.1111/j.1365-2486.2007.01365.x

Desai, A. R., Bolstad, P. V., Cook, B. D., Davis, K. J., & Carey, E. V. (2005). Comparing net ecosystem exchange of carbon dioxide between an old-growth and mature forest in the upper Midwest, USA. *Agricultural and Forest Meteorology*, *128*(1–2), 33–55. http://doi.org/10.1016/j.agrformet.2004.09.005

Digital Globe. (2013, June 3). Data Sheet WorldView-2. Retrieved from: https://dg-cms-uploads-production.s3.amazonaws.com/uploads/document/file/98/WorldView2-DS-WV2-rev2.pdf

Fugro Horizons, Inc. and the Minnesota Department of Natural Resources. (2015, March 10). LiDAR Elevation, Twin Cities Metro Region, Minnesota, 2011. Retrieved from: ftp://ftp.gisdata.mn.gov/pub/gdrs/data/pub/us_mn_state_mngeo/elev_lidar_metro2011/metadata/metadata.html

Gao, F., Masek, J., Schwaller, M., & Hall, F. (2006). On the blending of the Landsat and MODIS surface reflectance: Predicting daily landsat surface reflectance. *IEEE Transactions on Geoscience and Remote Sensing*, *44*(8), 2207–2218. http://doi.org/10.1109/TGRS.2006.872081

Goetz, S. J., & Prince, S. D. (1999). Modelling Terrestrial Carbon Exchange and Storage : Evidence and Implications of Functional Convergence in Light-use Efficiency. *Advances in Ecological Research*, *28*, 57–92.

Goulden, M. L., Daube, B. C., Fan, S.-M., Sutton, D. J., Bazzaz, A., Munger, J. W., & Wofsy, S. C. (1997). Physiological responses of a black spruce forest to weather. *Journal of Geophysical Research*, *102*(D24), 28987–28996. http://doi.org/10.1029/2007JG000640/abstract

Goulden, M. L., Winston, G. C., Mcmillan, A. M. S., Litvak, M. E., Read, E. L., Rocha, A. V., & Rob Elliot, J. (2006). An eddy covariance mesonet to measure the effect of forest age on land-atmosphere exchange. *Global Change Biology*, *12*(11), 2146–2162. http://doi.org/10.1111/j.1365-2486.2006.01251.x

Green, R. O., Eastwood, M. L., Sarture, C. M., Chrien, T. G., Aronsson, M., Chippendale, B. J., … Williams, O. (1998). Imaging spectroscopy and the Airborne Visible/Infrared Imaging Spectrometer (AVIRIS). *Remote Sensing of Environment*, *65*(3), 227–248. http://doi.org/10.1016/S0034-4257(98)00064-9

Grimm, N. B., Faeth, S. H., Golubiewski, N. E., Redman, C. L., Wu, J., Bai, X., & Briggs, J. M. (2008). Global change and the ecology of cities. *Science*, *319*(5864), 756–760. http://doi.org/10.1126/science.1150195

Hagishima, A., Narita, K. I., & Tanimoto, J. (2007). Field experiment on transpiration from isolated urban plants. *Hydrological Processes*, *21*(9), 1217–1222.

Ham, J. M., & Knapp, A. K. (1998). Fluxes of CO2 water vapor, and energy from a prairie ecosystem during the seasonal transition from carbon sink to carbon source. *Agricultural and Forest Meteorology*, *89*(1), 1–14.

Hardiman, B. S., Wang, J. A., Hutyra, L. R., Gately, C. K., Getson, J. M., & Friedl, M. A. (2017). Accounting for urban biogenic fluxes in regional carbon budgets. *Science of the Total Environment*, *592*, 366–372. http://doi.org/10.1016/j.scitotenv.2017.03.028

Heinsch, F. A., Running, S. W., Kimball, J. S., Nemani, R. R., Davis, K. J., Bolstad, P. V., … Flanagan, L. B. (2006). Evaluation of remote sensing based terrestrial productivity from MODIS using regional tower eddy flux network observations. *IEEE Transactions on Geoscience and Remote Sensing*, *44*(7), 1908–1925. http://doi.org/10.1109/TGRS.2005.853936

Heinsch, F. A., Reeves, M., Votava, P., Kang, S., Milesi, C., Zhao, M., … Running, S. W. (2003). *User's Guide GPP and NPP (MOD17A2/A3) products NASA MODIS Land Algorithm*. Retrieved from http://www.ncbi.nlm.nih.gov/pubmed/21564034

Herold, M., Gardner, M. E., & Roberts, D. A. (2003). Spectral resolution requirements for mapping urban areas. *IEEE Transactions on Geoscience and Remote Sensing*, *41*(9), 1907–1919. http://doi.org/10.1109/TGRS.2003.815238

Hiller, R. V., McFadden, J. P., & Kljun, N. (2011). Interpreting CO2 Fluxes Over a Suburban Lawn: The Influence of Traffic Emissions. *Boundary-Layer Meteorology*, *138*(2), 215–230. http://doi.org/10.1007/s10546-010-9558-0

Huete, A. R. (1988). A soil-adjusted vegetation index (SAVI). *Remote Sensing of Environment*, *25*(3), 295–309. http://doi.org/10.1016/0034-4257(88)90106-X

Huete, A., Didan, K., Miura, T., Rodriguez, E. P., Gao, X., & Ferreira, L. G. (2002). Overview of the radiometric and biophysical performance of the MODIS vegetation indices. *Remote Sensing of Environment*, *83*, 195–213. http://doi.org/10.1016/S0034-4257(02)00096-2

Imhoff, M. L., Tucker, C. J., Lawrence, W. T., & Stutzer, D. C. (2000). The use of multisource satellite and geospatial data to study the effect of urbanization on primary productivity in the United States. *IEEE Transactions on Geoscience and Remote Sensing*, *38*(6), 2549-2556.

Imhoff, M. L., Bounoua, L., DeFries, R., Lawrence, W. T., Stutzer, D., Tucker, C. J., & Ricketts, T. (2004). The consequences of urban land transformation on net primary productivity in the United States. *Remote Sensing of Environment*, *89*(4), 434–443. http://doi.org/10.1016/j.rse.2003.10.015

Imhoff, M. L., Zhang, P., Wolfe, R. E., & Bounoua, L. (2010). Remote sensing of the urban heat island effect across biomes in the continental USA. *Remote Sensing of Environment*, *114*(3), 504–513. http://doi.org/10.1016/j.rse.2009.10.008

Järvi, L., Nordbo, A., Junninen, H., Riikonen, A., Moilanen, J., Nikinmaa, E., & Vesala, T. (2012). Seasonal and annual variation of carbon dioxide surface fluxes in Helsinki, Finland, in 2006-2010. *Atmospheric Chemistry and Physics*, *12*(18), 8475–8489. http://doi.org/10.5194/acp-12-8475-2012

Jia, X., & Richards, J. A. (1994). Efficient maximum likelihood classification for imaging spectrometer data sets. *IEEE Transactions on Geoscience and Remote Sensing*, *32*(2), 274–281. http://doi.org/10.1109/36.295042

Keenan, T. F., Gray, J., Friedl, M. A., Toomey, M., Bohrer, G., Hollinger, D. Y., … Richardson, A. D. (2014). Net carbon uptake has increased through warming-induced changes in temperate forest phenology. *Nature Climate Change*, *4*(June), 598–604. http://doi.org/10.1038/NCLIMATE2253

Kim, J., & Hogue, T. S. (2012). Evaluation and sensitivity testing of a coupled Landsat-MODIS downscaling method for land surface temperature and vegetation indices in semi-arid regions. *Journal of Applied Remote Sensing*, *6*, 63569.

Kjelgren, R., & Montague, T. (1998). Urban tree transpiration over turf and asphalt surfaces. *Atmospheric Environment*, *32*(1), 35–41.

Kljun, N., Calanca, P., Rotachhi, M. W., & Schmid, H. P. (2004). A simple parameterisation for flux footprint predictions. *Boundary-Layer Meteorology*, *112*(3), 503–523.

Knyazikhin, Y., Glassy, J., Privette, J. L., Tian, Y., Lotsch, A., Zhang, Y., … Running, S. W. (1999). MODIS Leaf Area Index (LAI) And Fraction Of Photosynthetically Active Radiation Absorbed By Vegetation (FPAR) Product: Algorithm Theoretical Basis Document, *Version 4.*, 130. http://doi.org/http://eospso.gsfc.nasa.gov/atbd/modistables.html

Kordowski, K., & Kuttler, W. (2010). Carbon dioxide fluxes over an urban park area. *Atmospheric Environment*, *44*(23), 2722–2730. http://doi.org/10.1016/j.atmosenv.2010.04.039

Kurc, S. A., & Small, E. E. (2004). Dynamics of evapotranspiration in semiarid grassland and shrubland ecosystems during the summer monsoon season, central New Mexico. *Water Resources Research*, *40*(9), 1–15. http://doi.org/10.1029/2004WR003068

Lu, D., Xu, X., Tian, H., Moran, E., Zhao, M., & Running, S. (2010). The effects of urbanization on net primary productivity in southeastern China. *Environmental Management*, *46*(3), 404–410. http://doi.org/10.1007/s00267-010-9542-y

Ma, X., Huete, A., Yu, Q., Restrepo-Coupe, N., Beringer, J., Hutley, L. B., … Eamus, D. (2014). Parameterization of an ecosystem light-use-efficiency model for predicting savanna GPP using MODIS EVI. *Remote Sensing of Environment*, *154*, 253–271. http://doi.org/10.1016/j.rse.2014.08.025

Mahadevan, P., Wofsy, S. C., Matross, D. M., Xiao, X., Dunn, A. L., Lin, J. C., … Gottlieb, E. W. (2008). A satellite-based biosphere parameterization for net ecosystem CO2 exchange: Vegetation Photosynthesis and Respiration Model (VPRM). *Global Biogeochemical Cycles*, *22*(2). http://doi.org/10.1029/2006GB002735

McKinney, M. L. (2006). Urbanization as a major cause of biotic homogenization. *Biological Conservation*, *127*(3), 247–260. http://doi.org/10.1016/j.biocon.2005.09.005

Melaas, E. K., Wang, J. A., Miller, D. L., & Friedl, M. A. (2016). Interactions between urban vegetation and surface urban heat islands: a case study in the Boston metropolitan region. *Environmental Research Letters*, *11*(5), 54020. http://doi.org/10.1088/1748-9326/11/5/054020

Menzer, O., Meiring, W., Kyriakidis, P. C., & McFadden, J. P. (2015). Annual sums of carbon dioxide exchange over a heterogeneous urban landscape through machine learning based gap-filling. *Atmospheric Environment*, *101*, 312–327. http://doi.org/10.1016/j.atmosenv.2014.11.006

Metropolitan Council. (2011, August 24). Generalized Land Use 2010. Retrieved from: ftp://ftp.gisdata.mn.gov/pub/gdrs/data/pub/us_mn_state_metc/plan_generl_lnduse2010/metadata/metadata.html

Metropolitan Council. (2013, May 20). Lakes and Rivers – Open Water Features. Retrieved from: ftp://ftp.gisdata.mn.gov/pub/gdrs/data/pub/us_mn_state_metc/water_lakes_rivers/metadata/metadata.html

Metropolitan Council. (2016, June). The Twin Cities Regional Forecast to 2040: Steady Growth and Big Changes Ahead. Retrieved from: https://metrocouncil.org/Data-and-Maps/Publications-And-Resources/MetroStats/Land-Use-and-Development/The-Twin-Cities-Regional-Forecast-to-2040-Steady.aspx

Metropolitan Mosquito Control District (2012, May 30). Metro Wetlands and Wet Areas (MMCD).

Minnesota Department of Natural Resources and Surdex Corporation. (2015, February 4). Digital Orthoimagery, Twin Cities, Spring 2010, 1-ft Resolution. Retrieved from: http://www.mngeo.state.mn.us/chouse/metadata/ecmn2010_doqq_1ft.html

Meyers, T. P., & Hollinger, S. E. (2004). An assessment of storage terms in the surface energy balance of maize and soybean. *Agricultural and Forest Meteorology*, *125*(1–2), 105–115. http://doi.org/10.1016/j.agrformet.2004.03.001

Milesi, C., Elvidge, C. D., Nemani, R. R., & Running, S. W. (2003). Assessing the impact of urban land development on net primary productivity in the southeastern United States. *Remote Sensing of Environment*, *86*(3), 401–410. http://doi.org/10.1016/S0034-4257(03)00081-6

Milesi, C., Hashimoto, H., Running, S. W., & Nemani, R. R. (2005). Climate variability, vegetation productivity and people at risk. *Global and Planetary Change*, *47*(2–4 SPEC. ISS.), 221–231. http://doi.org/10.1016/j.gloplacha.2004.10.020

Monteith, J. L. (1972). Solar radiation and productivity in tropical ecosystems. *Journal of Applied Ecology*, *9*(3), 747–766.

Myeong, S., Nowak, D. J., Hopkins, P. F., & Brock, R. H. (2001). Urban cover mapping using digital, high-spatial resolution aerial imagery. *Urban Ecosystems*, *5*, 243–256. http://doi.org/10.1023/A:1025687711588

Myint, S. W., Gober, P., Brazel, A., Grossman-Clarke, S., & Weng, Q. (2011). Per-pixel vs. object-based classification of urban land cover extraction using high spatial resolution imagery. *Remote Sensing of Environment*, *115*(5), 1145–1161. http://doi.org/10.1016/j.rse.2010.12.017

Myneni, R. B., Hoffman, S., Knyazikhin, Y., Privette, J. L., Glassy, J., Tian, Y., … Running, S. W. (2002). Global products of vegetation leaf area and fraction absorbed PAR from year one of MODIS data. *Remote Sensing of Environment*, *83*(1–2), 214–231. http://doi.org/10.1016/S0034-4257(02)00074-3

Myneni, R. B., & Williams, D. L. (1994). On the relationship between FAPAR and NDVI. *Remote Sensing of Environment*, *49*(3), 200–211. http://doi.org/10.1016/0034-4257(94)90016-7

Noormets, A., Chen, J., & Crow, T. R. (2007). Age-Dependent Changes in Ecosystem Fluxes in Managed Forests in Northern Wisconsin, USA. *Ecosystems*, *10*(2), 187–203. http://doi.org/10.1007/sl0021-007-9018-y

Nordbo, A., Jarvi, L., Haapanala, S., Wood, C. R., & Vesala, T. (2012). Fraction of natural area as main predictor of net CO2 emissions from cities. *Geophysical Research Letters*, *39*.

Nouri, H., Beecham, S., Anderson, S., & Nagler, P. (2014). High spatial resolution WorldView-2 imagery for mapping NDVI and its relationship to temporal urban landscape evapotranspiration factors. *Remote Sensing*, *6*, 580–602. http://doi.org/10.3390/rs6010580

Novick, K. A., Stoy, P. C., Katul, G. G., Ellsworth, D. S., Siquiera, M. B. S., Juang, J., & Oren, R. (2004). Carbon dioxide and water vapor exchange in a warm temperate grassland. *Oecologia*, *138*, 259–274. http://doi.org/10.1007/s00442-003-1388-z

Nowak, D.J., 1994. Atmospheric carbon dioxide reduction by Chicago's urban forest. In: McPherson, E.G., Nowak, D.J., Rowntree, R.A. (Eds.), Chicago's Urban Forest Ecosystem: Results of the Chicago Urban Forest Climate Project. USDA Forest Service General Technical Report NE-186, Radnor, PA, pp. 83–94.

Nowak, D. J., & Crane, D. E. (2002). Carbon storage and sequestration by urban trees in the USA. *Environmental Pollution*, *116*(116), 381–389.

Nowak, D. J., Crane, D. E., Stevens, J. C., Hoehn, R. E., Walton, J. T., & Bond, J. (2008). A Ground-Based Method of Assessing Urban Forest Structure and Ecosystem Services. *Arboriculture & Urban Forestry*, *34*(6), 347–358.

Nowak, D. J., Crane, D. E., & Stevens, J. C. (2006). Air pollution removal by urban trees and shrubs in the United States. *Urban Forestry and Urban Greening*, *4*(3–4), 115–123. http://doi.org/10.1016/j.ufug.2006.01.007

Ogutu, B. O., & Dash, J. (2013). Assessing the capacity of three production efficiency models in simulating gross carbon uptake across multiple biomes in conterminous USA. *Agricultural and Forest Meteorology*, *174–175*, 158–169. http://doi.org/10.1016/j.agrformet.2013.02.016

Oke, T. R. (1989). The micrometeorology of the urban forest. *Philosophical Transactions of the Royal Society B: Biological Sciences*, *324*(1223), 335–349. http://doi.org/10.1098/rstb.1989.0051

Pataki, D. E., Alig, R. J., Fung, A. S., Golubiewski, N. E., Kennedy, C. A., Mcpherson, E. G., … Lankao, P. R. (2006). Urban ecosystems and the North American carbon cycle. *Global Change Biology*, *12*(11), 2092–2102. http://doi.org/10.1111/j.1365-2486.2006.01242.x

Pei, F., Li, X., Liu, X., Wang, S., & He, Z. (2013). Assessing the differences in net primary productivity between pre- and post-urban land development in China. *Agricultural and Forest Meteorology*, *171–172*, 174–186. http://doi.org/10.1016/j.agrformet.2012.12.003

Peters, E. B., & McFadden, J. P. (2012). Continuous measurements of net CO2 exchange by vegetation and soils in a suburban landscape. *Journal of Geophysical Research: Biogeosciences*, *117*, G03005.

Peters, E. B., & McFadden, J. P. (2010). Influence of seasonality and vegetation type on suburban microclimates. *Urban Ecosystems*, *13*(4), 443–460.

Peters, E. B., Hiller, R. V., & McFadden, J. P. (2011). Seasonal contributions of vegetation types to suburban evapotranspiration. *Journal of Geophysical Research: Biogeosciences*, *116*(1), 1–16. http://doi.org/10.1029/2010JG001463

Peters, E. B., McFadden, J. P., & Montgomery, R. A. (2010). Biological and environmental controls on tree transpiration in a suburban landscape. *Journal of Geophysical Research: Biogeosciences*, *115*(4), 1–13. http://doi.org/10.1029/2009JG001266

Potapenko, J. (2014). *High-Resolution LiDAR Pointcloud Data Processing, Computation, and Visualization with Application to the Erosion Analysis of the California Channel Islands*. University of California Santa Barbara.

Potter, S., Randerson, T., Field, B., Matson, A., Vitousek, P. M., Mooney, H. A., & Klooster, S. A. (1993). Terrestrial Ecosystem Production: A Process Model Based on Global Satellite and Surface Data. *Global Biogeochemical Cycles*, *7*(4), 811–841.

Pouyat, R. V, Yesilonis, I. D., & Nowak, D. J. (2006). Carbon storage by urban soils in the United States. *Journal of Environmental Quality*, *35*, 1566–1575.

Prince, S. D., & Goward, S. N. (1995). Global primary production: a remote sensing approach. *Journal of Biogeography*, *22*(4), 815–835.

Raciti, S. M., Hutyra, L. R., & Newell, J. D. (2014). Mapping carbon storage in urban trees with multi-source remote sensing data: Relationships between biomass, land use, and demographics in Boston neighborhoods. *Science of The Total Environment*, *500–501*, 72–83. http://doi.org/10.1016/j.scitotenv.2014.08.070

Reich, P. B. (2012). Key canopy traits drive forest productivity. *Proceedings of the Royal Society B: Biological Sciences*, *279*(1736), 2128–2134. http://doi.org/10.1098/rspb.2011.2270

Reinmann, A. B., & Hutyra, L. R. (2017). Edge effects enhance carbon uptake and its vulnerability to climate change in temperate broadleaf forests. *Proceedings of the National Academy of Sciences*, *114*(1), 107–112. http://doi.org/10.1073/pnas.1612369114

Roberts, D. A., Gardner, M., Church, R., Ustin, S., & Scheer, G. (1998). Mapping Chaparral in the Santa Monica Mountains Using Multiple Endmember Spectral Mixture Models. *Remote Sensing of Environment*, *65*, 267–279.

Ruimy, A., Saugier, B., & Dedieu, G. (1994). Methodology for the estimation of terrestrial net primary production from remotely sensed data. *Journal of Geophysical Research Atmospheres*, *99*, 5263–5283.

Running, S. W., Baldocchi, D. D., Turner, D. P., Gower, S. T., Bakwin, P. S., & Hibbard, K. A. (1999). A global terrestrial monitoring network integrating tower fluxes, flask sampling, ecosystem modeling and EOS satellite data. *Remote Sensing of Environment*, *70*(1), 108–127. http://doi.org/10.1016/S0034-4257(99)00061-9

Running, S. W., Nemani, R. R., Heinsch, F. A., Zhao, M., Reeves, M., & Hashimoto, H. (2004). A Continuous Satellite-Derived Measure of Global Terrestrial Primary Production. *BioScience*, *54*(6), 547. http://doi.org/10.1641/0006-3568(2004)054[0547:ACSMOG]2.0.CO;2

Running, S. W., & Zhao, M. (2015). User's Guide Daily GPP and Annual NPP (MOD17A2/A3) Products NASA Earth Observing System MODIS Land Algorithm Version 3.0 for Collection 6.

Schwalm, C. R., Black, T. A., Amiro, B. D., Arain, M. A., Barr, A. G., Bourque, C. P. a, … Wofsy, S. C. (2006). Photosynthetic light use efficiency of three biomes across an east-west continental-scale transect in Canada. *Agricultural and Forest Meteorology*, *140*(1–4), 269–286. http://doi.org/10.1016/j.agrformet.2006.06.010

Sen Roy, S., & Yuan, F. (2009). Trends in extreme temperatures in relation to urbanization in the Twin Cities metropolitan area, Minnesota. *Journal of Applied Meteorology and Climatology*, *43*(8), 669–679. http://doi.org/10.1175/2008JAMC1983.1

Seto, K. C., Güneralp, B., & Hutyra, L. R. (2012). Global forecasts of urban expansion to 2030 and direct impacts on biodiversity and carbon pools. *Proceedings of the National Academy of Sciences of the United States of America*, *109*(40), 16083–16088. http://doi.org/10.1073/pnas.1211658109

Sims, D. A., Luo, H. Y., Hastings, S., Oechel, W. C., Rahman, A. F., & Gamon, J. A. (2006a). Parallel adjustments in vegetation greenness and ecosystem CO2 exchange in response to drought in a Southern California chaparral ecosystem. *Remote Sensing of Environment*, *103*(3), 289–303.

Sims, D. A., Rahman, A. F., Cordova, V. D., El-Masri, B. Z., Baldocchi, D. D., Flanagan, L. B., … Xu, L. K. (2006b). On the use of MODIS EVI to assess gross primary productivity of North American ecosystems. *Journal of Geophysical Research-Biogeosciences*, *111*(G4).

Song, J., Liao, K., Coulter, R. L., & Lesht, B. M. (2005). Climatology of the low-level jet at the Southern Great Plains Atmospheric Boundary Layer Experiments site. *Journal of Applied Meteorology*, *44*, 1593–1606.

Song, C., Dannenberg, M. P., & Hwang, T. (2013). Optical remote sensing of terrestrial ecosystem primary productivity. *Progress in Physical Geography*, *37*(6), 834–854. http://doi.org/10.1177/0309133313507944

Spronken-Smith, R. A., Oke, T. R., & Lowry, W. P. (2000). Advection and the surface energy balance across an irrigated urban park. *International Journal of Climatology*, *20*(9), 1033-1047.

Still, C. J., Randerson, J. T., & Fung, I. Y. (2004). Large-scale plant light-use efficiency inferred from the seasonal cycle of atmospheric CO2. *Global Change Biology*, *10*, 1240–1252. http://doi.org/10.1111/j.1365-2486.2004.00802.x

Strohbach, M. W., & Haase, D. (2012). Above-ground carbon storage by urban trees in Leipzig, Germany: Analysis of patterns in a European city. *Landscape and Urban Planning*, *104*(1), 95–104. http://doi.org/10.1016/j.landurbplan.2011.10.001

Todhunter, P. E. (1996). Environmental indices for the Twin Cities Metropolitan Area (Minnesota, USA) urban heat island - 1989. *Climate Research*, *6*(1), 59–69.

Tucker, C. J. (1979). Red and photographic infrared linear combinations for monitoring vegetation. *Remote Sensing of Environment*, *8*(2), 127–150. http://doi.org/10.1016/0034-4257(79)90013-0

Turner, D. P., Ritts, W. D., Cohen, W. B., Gower, S. T., Running, S. W., Zhao, M., … Ahl, D. E. (2006). Evaluation of MODIS NPP and GPP products across multiple biomes. *Remote Sensing of Environment*, *102*(3–4), 282–292. http://doi.org/10.1016/j.rse.2006.02.017

Turner, D. P., Ritts, W. D., Cohen, W. B., Gower, S. T., Zhao, M., Running, S. W., … Munger, J. W. (2003a). Scaling Gross Primary Production (GPP) over boreal and deciduous forest landscapes in support of MODIS GPP product validation. *Remote Sensing of Environment*, *88*(3), 256–270. http://doi.org/10.1016/j.rse.2003.06.005

Turner, D. P., Ritts, W. D., Cohen, W. B., Maeirsperger, T. K., Gower, S. T., Kirschbaum, A. A., … Gamon, J. A. (2005). Site-level evaluation of satellite-based global terrestrial gross primary production and net primary production monitoring. *Global Change Biology*, *11*, 666–684. http://doi.org/10.1111/j.1365-2486.2005.00936.x

Turner, D. P., Urbanski, S., Bremer, D., Wofsy, S. C., Meyers, T., Gower, S. T., & Gregory, M. (2003b). A cross-biome comparison of daily light use efficiency for gross primary production. *Global Change Biology*, *9*(3), 383–395. http://doi.org/10.1046/j.1365-2486.2003.00573.x

Velasco, E., & Roth, M. (2010). Cities as net sources of CO2: Review of atmospheric CO2 exchange in urban environments measured by eddy covariance technique. *Geography Compass*, *4*(9), 1238–1259. http://doi.org/10.1111/j.1749-8198.2010.00384.x

Verma, M., Friedl, M. A., Law, B. E., Bonal, D., Kiely, G., Black, T. A., … D'Odorico, P. (2015). Improving the performance of remote sensing models for capturing intra- and inter-annual variations in daily GPP: An analysis using global FLUXNET tower data. *Agricultural and Forest Meteorology*, *214–215*, 416–429. http://doi.org/10.1016/j.agrformet.2015.09.005

Verma, M., Friedl, M. A., Richardson, A. D., Kiely, G., Cescatti, A., Law, B. E., … Propastin, P. (2014). Remote sensing of annual terrestrial gross primary productivity from MODIS: An assessment using the FLUXNET la Thuile data set. *Biogeosciences*, *11*(8), 2185–2200. http://doi.org/10.5194/bg-11-2185-2014

Walton, J. T., Nowak, D. J., & Greenfield, E. J. (2008). Assessing Urban Forest Canopy Cover Using Airborne or Satellite Imagery. *Arboriculture & Urban Forestry*, *34*(6), 334–340.

Waring, R. H., Landsberg, J. J., & Williams, M. (1998). Net primary production of forests: a constant fraction of gross primary production? *Tree Physiology*, *18*(2), 129–134. http://doi.org/10.1093/treephys/18.2.129

Wetherley, E. B., Roberts, D. A., & McFadden, J. P. (2017). Mapping spectrally similar urban materials at sub-pixel scales. *Remote Sensing of Environment*, *195*, 170–183. http://doi.org/10.1016/j.rse.2017.04.013

Winkler, J. A., Skaggs, R. H., & Baker, D. G. (1981). Effect of temperature adjustments on the Minneapolis-St. Paul urban heat island. *Journal of Applied Meteorology*, *20*, 1295–1300.

Wofsy, S. C., Goulden, M. L., Munger, J. W., Fan, S.-M., Bakwin, P. S., Daube, B. C., … Bazzaz, F. A. (1993). Net Exchange of CO2 in a Mid-Latitude Forest. *Science*, *260*, 1314–1317. http://doi.org/10.1029/2007JG000640/abstract

Woodcock, C. E., & Strahler, A. H. (1987). The factor of scale in remote sensing. *Remote Sensing of Environment*, *332*(21), 311–332. http://doi.org/10.1016/0034-4257(87)90015-0

Wu, C., Chen, J. M., Desai, A. R., Hollinger, D. Y., Arain, M. A., Margolis, H. A., … Staebler, R. M. (2012). Remote sensing of canopy light use efficiency in temperate and boreal forests of North America using MODIS imagery. *Remote Sensing of Environment*, *118*, 60–72. http://doi.org/10.1016/j.rse.2011.11.012

Wu, J., & Bauer, M. E. (2012). Estimating net primary production of turfgrass in an urban-suburban landscape with QuickBird imagery. *Remote Sensing*, *4*(4), 849–866. http://doi.org/10.3390/rs4040849

Xiao, J., Zhuang, Q., Law, B. E., Chen, J., Baldocchi, D. D., Cook, D. R., … Wofsy, S. C. (2010). A continuous measure of gross primary production for the conterminous United States derived from MODIS and AmeriFlux data. *Remote Sensing of Environment*, *114*(3), 576–591. http://doi.org/10.1016/j.rse.2009.10.013

Xiao, X., Hollinger, D., Aber, J., Goltz, M., Davidson, E. A., Zhang, Q., & Moore, B. (2004). Satellite-based modeling of gross primary production in an evergreen needleleaf forest. *Remote Sensing of Environment*, *89*, 519–534. http://doi.org/10.1016/j.rse.2003.11.008

Xu, C., Liu, M., An, S., Chen, J. M., & Yan, P. (2007). Assessing the impact of urbanization on regional net primary productivity in Jiangyin County, China. *Journal of Environmental Management*, *85*(3), 597–606. http://doi.org/10.1016/j.jenvman.2006.08.015

Yang, F., Ichii, K., White, M. A., Hashimoto, H., Michaelis, A. R., Votava, P., … Nemani, R. R. (2007). Developing a continental-scale measure of gross primary production by combining MODIS and AmeriFlux data through Support Vector Machine approach. *Remote Sensing of Environment*, *110*(1), 109–122. http://doi.org/10.1016/j.rse.2007.02.016

Yuan, F., Sawaya, K. E., Loeffelholz, B. C., & Bauer, M. E. (2005). Land cover classification and change analysis of the Twin Cities (Minnesota) Metropolitan Area by multitemporal Landsat remote sensing. *Remote Sensing of Environment*, *98*(2–3), 317–328.

Yuan, W., Liu, S., Zhou, G., Zhou, G., Tieszen, L. L., Baldocchi, D., … Wofsy, S. C. (2007). Deriving a light use efficiency model from eddy covariance flux data for predicting daily gross primary production across biomes. *Agricultural and Forest Meteorology*, *143*, 189–207. http://doi.org/10.1016/j.agrformet.2006.12.001

Zhang, Y., Song, C., Sun, G., Band, L. E., McNulty, S., Noormets, A., … Zhang, Z. (2016). Development of a coupled carbon and water model for estimating global gross primary productivity and evapotranspiration based on eddy flux and remote sensing data. *Agricultural and Forest Meteorology*, *223*, 116–131. http://doi.org/10.1016/j.agrformet.2016.04.003

Zhao, T., Brown, D. G., & Bergen, K. M. (2007). Increasing Gross Primary Production (GPP) in the Urbanizing Landscapes of Southeastern Michigan. *Photogrammetric Engineering & Remote Sensing*, *73*(10), 1159–1167.

Zhao, T., Brown, D. G., Fang, H., Theobald, D. M., Liu, T., & Zhang, T. (2012). Vegetation productivity consequences of human settlement growth in the eastern United States. *Landscape Ecology*, *27*(8), 1149–1165. http://doi.org/10.1007/s10980-012-9766-8